ISTANBUL TECHNICAL UNIVERSITY ★ GRADUATE SCHOOL OF SCIENCE ENGINEERING AND TECHNOLOGY

DESIGN AND REALIZATION OF A SPECKLE ENHANCED PRISM SPECTROMETER

M.Sc. THESIS

Şakir Kaan ÇETİNDAĞ

Department of Electronics and Communication Engineering

Biomedical Engineering Programme

October 2018

ISTANBUL TECHNICAL UNIVERSITY ★ GRADUATE SCHOOL OF SCIENCE ENGINEERING AND TECHNOLOGY

DESIGN AND REALIZATION OF A SPECKLE ENHANCED PRISM SPECTROMETER

M.Sc. THESIS

Şakir Kaan ÇETİNDAĞ
504151417

Department of Electronics and Communication Engineering

Biomedical Engineering Programme

Thesis Advisor: Assistant Prof. Onur FERHANOĞLU

October 2018

ISTANBUL TEKNİK ÜNİVERSİTESİ ★ FEN BİLİMLERİ ENSTİTÜSÜ

BENEK DESENLERİ İLE GELİŞTİRİLMİŞ PRİZMA SPEKTROMETRESİ TASARIMI VE GERÇEKLENMESİ

YÜKSEK LİSANS TEZİ

Şakir Kaan ÇETİNDAĞ
504151417

Elektronik ve Haberleşme Mühendisliği Anabilim Dalı

Biyomedikal Mühendisliği Programı

Tez Danışmanı: Yrd. Doç. Dr. Onur FERHANOĞLU

October 2018

Ş. Kaan Çetindağ, a M.Sc. student of İTU Graduate School of Science Engineering and Technology student ID 504151417, successfully defended the thesis/dissertation entitled "DESIGN AND REALIZATION OF A SPECKLE ENHANCED PRISM SPECTROMETER" which he prepared after fulfilling the requirements specified in the associated legislations, before the jury whose signatures are below.

Thesis Advisor :	**Asst. Prof. Onur FERHANOĞLU** İstanbul Technical University	.....
Jury Members :	**Prof. Dr. Name SURNAME** Istanbul Technical University	.....
	Prof. Dr. Name SURNAME ..... University	.....
	Prof. Dr. Name SURNAME ..... University	.....

Date of Submission : 04 October 2018
Date of Defense : 26 October 2018

To my family,

FOREWORD

I would like to extend my deepest thanks and gratitude to my academic advisor Dr. Onur Ferhanoğlu and Dr. Fehmi Çivitçi for their invaluable support and guidance throughout my thesis. I would also like to acknowledge Dr. M. Fatih Toy for his valuable inputs. I would also like to thank members of Electro-Optic Devices Laboratory (EDL), my family and my friends.

Finally, special thanks to the Scientific and Technological Research Council of Turkey (TIBITAK) for supporting this work under grant 116F142 and 215E259.

October2018

Şakir Kaan Çetindağ
Electric & Electronics Engineer

TABLE OF CONTENTS

Page

ABBREVIATIONS

1D **:** 1-Dimensional
2D **:** 2-Dimensional
3D **:** 3-Dimensional
CCD **:** Charged Coupled Device
DR **:** Dynamic Range
FWHM **:** Full Width Half Maximum
HWHM **:** Half Width Half Maximum
NIR **:** Near Infrared
OCT **:** Optical Coherence Tomography
SLD **:** Super Luminescent Diode

SYMBOLS

n	**:** Number of spatial channels
m	**:** Number of spectral channels
$\boldsymbol{\sigma_e}$	**:** Experimental noise
$\boldsymbol{\tau}$	**:** Mean speckle intensity
$\boldsymbol{\lambda}$	**:** Wavelength
$\boldsymbol{\lambda_c}$	**:** Central wavelength
$\Delta\boldsymbol{\lambda}$	**:** Wavelength Step
$\Delta\boldsymbol{\Lambda}$	**:** Wavelength Range

LIST OF TABLES

Page

LIST OF FIGURES

Page

DESIGN AND REALIZATION OF A SPECKLE ENHANCED PRISM SPECTROMETER

SUMMARY

Spectroscopy is an application which uses the interaction of matter with electromagnetic waves. This interaction is quantified as radiation intensity as a function of wavelength. A series of different methods are used to measure the distribution of wavelengths inside the electromagnetic radiation.

One of these methods is the grating based spectrometer, which uses the diffraction of light to separate the different wavelength components inside the incoming electromagnetic waves. Periodic patterns of fringes are created on the imaging plane depending on the wavelength, which can be used to measure the intensity of each component by analysing the fringe intensities. Grating spectrometers have a high resolution but because fringes can overlap, its free spectral range is very limited.

Prism, with its dispersive nature is also a common tool used in spectrometer design. As light passes through a prism, different wavelength components propagate in different ways, resulting in separation of different components. The separated wavelength components illuminate different parts of the detector and thus spectroscopy is achieved. Because the propagation direction of different wavelength components do not overlap, the prism has an infinite free spectral range.

Speckle spectrometry has arisen as a new and promising alternative to spectral-spatial mapping, where each wavelength is mapped to a different speckle pattern on the detector rather than being mapped on different regions on the detector. Various methods exist to generate speckle patterns on the detector, which is generally a CMOS or CCD camera.

One example method for speckle generation is the use of multimode fibers. As the light propagates through the fiber optic cable, the modes inside the fiber interact and interfere with each other. This in turn creates a speckle pattern at the exit of the fiber optic cable. The length and diameter of the fiber optic cable determines the properties of the speckle pattern such as its shape and size.

Another example is the usage of scattering media. As a coherent light beam enters the scattering media, the coherence is disrupted by the random interactions of particles and photons. This causes the exiting incoherent light to generate a speckle pattern in the image plane. The thickness and substance of the used scattering medium affect the properties of the speckle pattern.

In both cases the properties of the resulting speckle pattern also depends on the wavelength of the propagating light. Generating speckle patterns, in this way, create a 1D-to-2D mapping from the spectrum space to spatial space. Knowing the physical properties of the speckle generation pattern, this dependency can be used to detect the wavelength of the light wave by analyzing the speckle patterns.This thesis investigates

the use of a scattering medium generated speckle pattern as an enhancement to a prism and realizes a spectrometer based on joint use of a prism and a scattering medium.

The scattering medium is placed between two cylindrical lenses, which first focuses the light onto the scattering medium as a line, and the second one collimates the created speckle pattern onto the prism. The dispersed speckle pattern exiting the prism is then focused onto the detector – a CCD camera – with another cylindrical lens.

Integrating a scattering medium and in this way speckle patterns into the system allows the prism to map every speckle pattern created by a different wavelength component to a different position in the detector. The formed speckle pattern secures a significant improvement in the resolution (up to x50 demonstrated) as opposed to the absence of the scattering medium.

Since the exact physical properties of the scattering medium cannot be known precisely, a calibration step is necessary in the spectrometer application. A tunable laser is used to sweep through a wavelength interval, recording the generated speckle patterns of each single wavelength (Eigen-functions). These recorded speckle patterns are then used to reconstruct any input, which is a linear combination of the calibration patterns used by determining the weight (Eigen-values) of each speckle pattern component inside the input.

With the proposed spectrometer, implemented using a simple CCD camera, a resolution of 17 pm was achieved with 750 nm wavelength range revealing a dynamic range of ~45,000. The dynamic range could be further improved upon using a detector array having larger area (to increase wavelength range) and a more scattering medium (to improve wavelength resolution). With further development, the proposed device could be useful in a variety of spectroscopy applications such as detailed delineation of retinal layers in Optical Coherence Tomography.

BENEK DESENLERİ İLE GELİŞTİRİLMİŞ PRİZMA SPEKTROMETRESİ TASARIMI VE GERÇEKLENMESİ

ÖZET

Spektroskopi elektromanyetik dalgaların madde ile etkileşimini kullanarak ölçüm yapma işlemi olup, günümüde biyomedikalden inşaate (çimento karışımlarının yoğunluk ölçümü) bir çok sektörde sıkça kullanılmaltadır. Elektromanyetik radyasyonun madde ile etkileşimi sonrası dalgaboyunda meydana gelen değişiklikler bir spektrometre ile incelenerek madde hakkında bilgi sahibi olunur ve bu sayede hızlı ve kesin sonuçlar elde edilir. Spektrometreler çalışma prensiplerine göre gruplandırılabilir.

Prizma spektrometreleri ışığın kırılmasını kullanarak gelen elektromanyetik dalgayı dalga boylarına göre ayırır. Elektromanyetik dalgalar yayılma sırasında ortam değiştirdiğinde kırılmaya uğrar ve yön değiştirir. Bu kırılma açışı ortamların kırılma indisleri oranına, dolayısıyla da prizmayapımında da kullanılan malzemeye ve gelen elektromanyetik dalganın dalga boyuna bağlıdır. Geniş dalga boyuna sahip elektromanyetik dalgalar daha fazla kırılırken küçük dalga boyuna sahip olanlar daha kırılmaya uğrar. Bu sayede farklı açılarda yayılmaya devam ederler ve ayrılmış olurlar.

Kırılma açısı dalga boyları arasındaki farka bağlı olduğu için küçük dalga boyu farkı küçük kırılma açısı farkı yaratacaktır. Bu da prizma spektrometrelerinin çözünürlüğünü kullanılan prizmanın malzemesine ve boyutuna bağlı bir hale getirmekte ve dolayısıyla çok yüksek çözünürlüklü prizma spektrometrelerin gerçekleştirilmesini zorlaştırmaktadır.

Kırınım ızgarası spektrometreleri ise elektromanyetik dalgaları kırınımı kullanarak dalga boylarına ayırırlar. Kırınım ızgarasında her bir delik farklı bir ışık kaynağı gibi davranacağı için bu kaynaklardan çıkan ışıklar ekran üzerinde girişim deseni oluşturmaktadır. Bu girişim desenleri dalgaboyu aralığı arttıkça üst üste bineceklerinden dolayı kırınım ızgaralarının kullanılabileceği dalga boyu aralığı genellikle sınırlıdır.

Üçüncü ve diğer iki metoda kıyasla daha yeni sayılabilecek bir başka spektrometre dizaynı da benek (speckle) desenlerini kullanarak elektromanyetik dalganın dalga boyu değişimlerini inceler. Koherent elektromanyetik dalga koherensini kaybetmesi sonucunda kendi içinde girişime uğraması sonucunda benek desenleri oluşur.

Elektromanyetik dalganın koherensini kaybetmesine yol açan birden fazla yöntem vardır. Bunlardan bir tanesi elektromanyetik dalganın çok kipli bir fiber optik kablodan geçmesi ve farklı kiplerin birbiriyle girişip kablo çıkışında benek desenleri oluşmasıdır.

Bir diğer yöntem de elektromanyetik dalganın dağıtıcı bir yüzeyden geçerken dalga boyuna bağlı olarak pseudorandom bir şekilde saçılması ve bunun sonucunda saçılan farklı dalga boyu elemanlarının girişime uğramasıyla benek desenlerinin oluşmasıdır.

Her iki durumda da oluşan benek desenleri koherensi bozan fiziksel ortamın özelliklerininyanı sıra kullanılan elektromanetik dalganın dalga boyuna bağlıdır ve bu sebeple oluşan benek desenleri bir CMOS veya CCD kamera ile kaydedilip incelenerek dalga boyu hakkında bilgi vermektedir ve bu sayede benek desenleri de bir spektrometre olarak kullanılabilmektedir.

Benek desenleri kullanılarak gerçeklenen bir spektrometrenin hem prizma hem de kırınım ızgarası spektrometrelerine kıyazla avantajları vardır. Prizma spektrometreleri geniş bir serbest spektral alana sahipken düşük çözünürlük sağlamaktadırlar ve kırınım ızgarası spektrometreleride yüksek çözünürlüğe sahip olmalarına karşın serbest spektral alanları dardır.

Benek deseni spektrometreleri ise her iki spektrometreden daha yüksek bir çözünürlüğe sahiptirler. Bunun sebebi benek spektrometrelerinin bir boyutlu dalga boyu uzayını diğer spektrometrelerin aksine iki boyutlu uzamsal uzaya haritalamalarıdır.

Bu tezde bir prizma ile saçıcı beraber kullanılarak benek ile geliştirilmiş bir prizma spektrometresi (SEPS) tasarlanmış ve gerçeklenmiştir. Saçıcının prizma ile beraber kullanılması prizmanın geniş – teorik olarak sonsuz – serbest spektral alanını benek desenlerinin yüksek çözünürlüğü ile birleştirmektedir.

Sistem elektromanyetik dalgayı önce silindirik lens yardımıyla bir saçıcıya odaklayıp daha sonra yine bir silindirik lens yardımıyla paralelleştirip prizmadan geçirmekedir. Prizmadan sonra da tekrar bir silindirik lens ile CCD kameraya odaklamaktadır. Bu sayede saçının çıkışında oluşan farklı dalga boylarına bağlı farklı benek desenleri prizmadan geçerken farklı bir kırılma açısıyla kırılacakları için kamera üzerinde farklı bir alana düşmektedirler. Bu gerçeklenen spektrometrenin teorik olarak sonsuz olan serbest spektral alanını kullanılan kameranın sensör alanının genişliği ile sınırlandırmaktadır.

Oluşan benek desenleri kullanılan saçıcının kalınlığı, konsantrasyonu ve homojenitesi gibi fiziksel özelliklerine bağlıdır. Bu özelliklerin yüksek bir hassasiyet ile bilinmesi mümkün olmamakla birlikte bilinse dahi oluşacak benek desenlerinin önceden hesaplanması oldukça zordur. Ayrıca sistemin tamamında oluşacak en ufak bir değişiklik (sıcaklık değişimi veya mekanik bir değişiklik) tüm hesaplamalrı değiştirecektir. Bu sebeble SEPS'in çalışma prensibi öncelikle sistemin kalibrasyonuna dayanmaktadır.

Kalibrasyon aşamasında dalga boyu ayarlanabilir bir lazer ışık kaynağı kullanılarak sistemin farklı dalga boylarında oluşturduğu benek desenleri kamera ile kaydedilmektedir. Bu aşamada kaydedilen benek desenleri daha sonra sisteme girdilerin geri çatımında kullanılmaktadır. Sistem girdi olarak kalibrasyon aşamasında kullanılan dalga boylarının herhangi bir lineer kombinasyonunu geri çatabilir.

Bu çalışmada kullanılan dalga boyu ayarlanabilir lazer kaynağının dalga boyu aralığı 830-850 nm arasındadır ve 10 pm adımlarla bu aralığı taramak mümkündür. Böylece sistemin çözünürlük sınırı 10 pm, serbest spektral alan sınırı ise 50 nm'dir.

Sistem birden fazla saçıcı ile kalibre edilmiş ve her birininin farklı bir çözünürlük değerine sahip olduğu gözlenmiştir. Saçıcı olarak fırın kağıdı, eskiz kağıdı gibi kolay ulaşılabilir malzemelerin yanı sıra TiO_2 (Titanyum Dioksit) nanoparçacıklarının epoksi içinde kurutulmasıyla üretilen saçıcılar da kullanılmıştır. Bu saçıcıların farklı kalınlık ve konsantrasyon kombinasyonları da denenmiştir. Bunun sonucunda beklendiği üzere en kalın ve en çok TiO_2 yoğunluğu bulunduran saçıcılar en yüksek

çözünürlük değerlerini vermişlerdir fakat bunun yanında geçirgenlikleri de fazlasıyla düştüğü için geçirgenlik ve çözünürlüğü optimize eden saçıcıyla spektrometrenin yapımına devam edilmiştir.Kullanılan saçıcı 750 um kalınlığında olup içindeki TiO2 epoksi oranı 1/12'dir. Kullanılan bu saçıcı ile 17 pm çözünürlüğe ulaşılmıştır.

Spektrometrenin dinamik aralığı oluşan benek desenlerinin CCD kamera üzerinde kapladığı alanla ters orantılı olup bu alan saçıcı arkasına bir yarık konularak küçültülebilir ve bu sayede dinamik aralık arttırılabilir.

Sistemde kullanılan saçıcı arkasına 50 um genişliğinde bir yarık konulmuş ve bu sayede oluşan benek deseninin kamera üzerinde kapladığı alanın genişliği de 20 piksele denk gelicek şekilde inceltilmiştir. Bunun sonucunda yatay eksende 1392 piksel bulunan CCD kamera ile 45000 dinamik aralığa ulaşılmıştır.

Tasarlanan bu sistem ile yüksek çözünrülüklüö geniş serbest spektral alanlı ve ultra yüksek dinamik aralıklı bir spektrometre gerçeklenmiştir.

1. INTRODUCTION

1.1 Motivation

Spectroscopy spans a wide range of applications, including identification of proteins in biology [1], material characterization [2], telecommunication [3], opto-medical imaging (such as Optical Coherence Tomography or shortly OCT) [4], and many others [5]. Thanks to its simplicity and efficacy, spectral-spatial mapping is among the most common used techniques in spectroscopy, wherein every wavelength component is mapped to different spatial position. Conventionally, spectral-spatial mapping is achieved with either one of the optical components, namely i) diffraction gratings, or ii) prisms. Although diffraction grating spectrometers typically offer a superior resolution over prism-based spectrometers, they are limited in their wavelength-range (free-spectral range) due to overlapping of diffracted orders [6].

Speckle spectrometry has arisen as a new and promising alternative to spectral-spatial mapping, where each wavelength is mapped to a different speckle pattern on the detector array rather than being mapped on different regions on the detector. The reconstruction is performed through first recording the patterns (Eigen-functions) of each wavelength through utilizing a tunable light source, and then finding the weights of the recorded patterns (Eigen-values) within the captured image for a broadband source. The differing speckle patterns imaged on a camera can be seen in Figure 1.1.

This work, by combining a prism and a scattering medium, which generates speckle patterns, aims to alleviate the trade off between the spectral range and resolution of a spectrometer, this way enabling an easier adoption of spectroscopy in multiple fields.

Speckle spectrometers allow for a higher wavelength range due to spatial-to-spectral mapping occurring as speckle patterns, allowing for a 2D mapping instead of locations on a detector array, which is inherently 1D. Yet, implementations of speckle spectrometer are typically fiber-based and display a very limited wavelength- range [7-9]. This is due to limited mode counts on the fiber optic cable.

Another implementation involves deploying ordered or random particles onto a substrate and collecting the scattered light into pre fabricated channels on the substrate. Instead of a sensor array, light is incident on different channels and the relative intensities of these channels are used to reconstruct the spectrum [10].

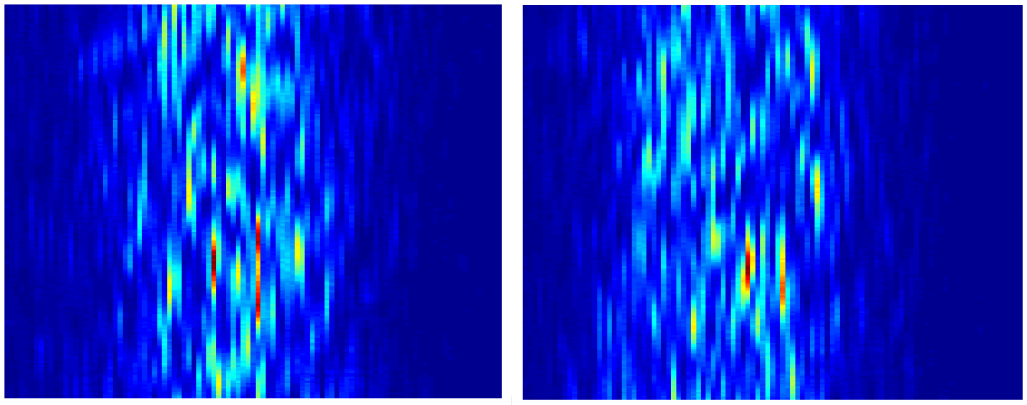

Figure 1.1: Speckle change for $\Delta\lambda$=1 nm

A free-air speckle spectrometry demonstration also exists, using the reflection from an optically rough surface with an oblique angle, achieving a resolution of 100MHz [11]

1.2 Purpose of Thesis

The purpose of this thesis is to design and realize a hybrid spectrometer based on speckle pattern analysis. The designed spectrometer employs both a scattering medium for speckle generation and a prism to, simultaneously achieve wide range and high resolution (thus high dynamic range), hence the name of the spectrometer is Speckle Enhanced Prism Spectrometer (SEPS). SEPS embarks both spectral-spatial mapping and speckle elements; it is essentially an improved type of prism spectrometer with significantly enriched resolution.

1.3 Hypothesis

In this thesis, enhancement of a prism spectrometer by employing a scattering medium to generate speckle patterns is proposed. It is hypothesized and experimentally proven that a better resolution and spectral range can be achieved compared to stand-alone prism spectrometers, diffraction grating spectrometers and previously published

speckle spectrometers. The proposed spectrometer architecture is named Speckle Enhanced prism Spectrometer (SEPS).

2. SPECTROMETERS

An optical spectrometer is an instrument that is used to measure properties of electromagnetic radiation, typically to identify materials in spectroscopic analysis [12]. The measured variable is often the intensity of the light but could also be the polarization state [13] and the independent variable is generally the wavelength.

Joseph von Fraunhofer developed the first spectrometer by combining a prism with a diffraction slit and telescope, which increased the spectral resolution. The first diffraction spectroscope was also invented by Fraunhofer [14].

2.1 Prism Spectrometers

As one of the oldest methods for spectrometry, the working principle of prism spectrometers depend on refraction due to dispersion. Dispersion is the dependency of the phase velocity of the electromagnetic wave to its wavelength. When an electromagnetic wave enters a dispersive media, it changes direction, which is called refraction. Different wavelengths are refracted in different refraction angles and this refraction angle depends on the refractive index (n) of the two mediums.

Refractive index is a number that represents how light propagates through a given medium and is defined as:

$$n = \frac{c}{v_p} \tag{2.1}$$

where c is the speed of light in vacuum and v_p is the phase velocity of light in a given medium. The phase velocity changes due to changes in dielecetric constant(ϵ) and magnetic moment(μ), and since frequency remains constant to satisfy the boundary conditions, this change is due to change in the wavelength of the light[15]. This makes the refraction index of a medium dependent on the wavelength of the propagating light and this dependency can be found empirically by using the Sellmeier equation:

$$n(\lambda) = \sqrt{1 + \sum_i \frac{B_i \lambda^2}{\lambda^2 - C_i}} \tag{2.2}$$

where B_i and C_i are experimentally determined Sellmeier coefficients of a given material[1] and λ is the vacuum wavelength in micrometers.

The difference in refraction angles can be calculated using the Snell's Law, which states that:

$$\frac{n_1}{n_2} = \frac{\sin\theta_2}{\sin\theta_1} \tag{2.3}$$

where n_1 and n_2 are the refraction indeces of two media and θ_1 and θ_2 are the incident and refraction angles, respectively. Solving equation 2.3 for two different wavelengths λ_1, λ_2 with the same n_1, θ_1 and dispersive media refractive indeces $n_2(\lambda_1)$ and $n_2(\lambda_1)$ from equation 2.2, we can get the respective refraction angles.

In prism spectrometers the effective separation of different wavelength components occur when the propagating light exits the prism and its measured by the angle of deviation, which can be seen in Figure 2.1.

In Figure 2.1., θ_i and θ_e are angle of incidence and angle of emergence repectively and A is the prism angle. To calculate the angle of deviation δ, we need to apply Snell's Law at both the incident and emergence point and write θ_e in terms of θ_i, which yields:

$$\delta(\theta_i) = \theta_i - A + \sin^{-1}(n(\lambda)\sin(A - \sin^{-1}(\frac{\sin\theta_i}{n(\lambda)}))) \tag{2.4}$$

It should be noted that since an incoming light will not have different incident angles for different wavelength components and the prism angle A is constant, the main factor determining the deviation angle is the term $n(\lambda)$. Thus, the wavelength seperation in prism spectrometer operation depends only on $n(\lambda)$. Table 2.1 shows three commonly used optic materials and their respective refractive indeces for two wavelengths, namely λ_1=850 nm and λ_2=851 nm.

As it can be seen from the table, the change in refractive index and the deviation angle between the two wavelengths that are one nm apart is extremely small, leading to a limited resolution in prism spectrometers.

[1] Sellmeier coefficients for most of the optical materials with many other properties can be found in refactiveindex.info

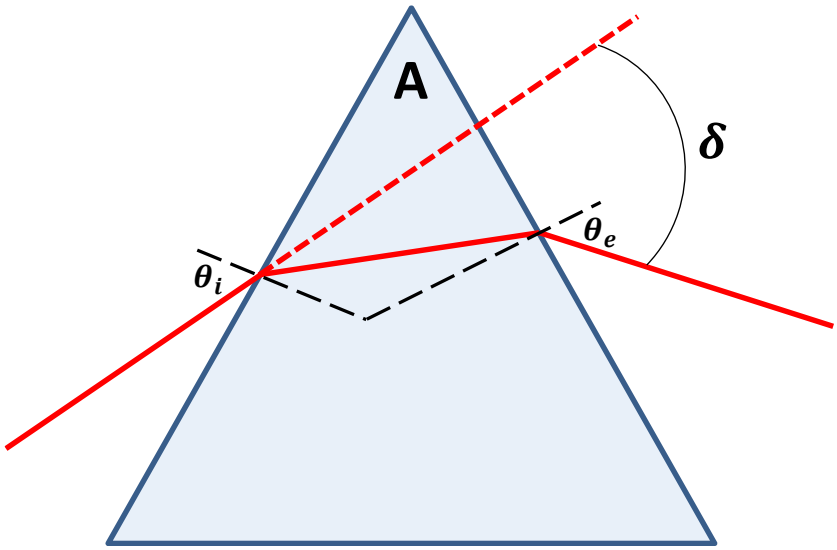

Figure 2.1: Prism angle of deviation.

Although limited in resolution, the free spectral range of prism spectrometers, which is the wavelength range that the spectrometer can be used in, is theoretically infinite. This is due to the refraction index dependency to wavelength, which maps each wavelength component into a unique deviation angle, no matter the range.

The usage of prism spectrometer in SEPS is based on this fact, and the prism employed in the system allows the free spectral range of the proposed spectrometer to be theoretically infinite.

2.2 Grating Spectrometers

Grating spectrometers are another widely used form of spectrometers, which employ a diffraction grating to separate an incoming light into its wavelength components. A diffraction grating is a periodic structure that diffracts light into several beams travelling in different direction, depending on their wavelength.

Diffraction can be described by the Huygens-Fresnel principle, which models the propagation of light as a combination of spherical wavelets created by point sources on the wave front, and the superposition principle of light [16].

When light passes through a diffraction grating, which possesses multiple slits for light to pass through, each of these slits acts like another light source and they interfere through their propagation.

Table 2.1: Refractive index and deviation angle of common glass materials for $\boldsymbol{\lambda_1}$=850 nm and $\boldsymbol{\lambda_2}$=851 nm.

Material	Refractive Index ($\boldsymbol{\lambda_1}$=850nm)	Deviation Angle ($\boldsymbol{\theta_i = 50^\circ}$)	Refractive Index ($\boldsymbol{\lambda_2}$=851nm)	Deviation Angle ($\boldsymbol{\theta_i = 50^\circ}$)
N-BK7	1.50984	38.0510	1.50982	38.0495
Flint	1.60677	47.1567	1.60674	47.1536
SF11	1.76192	72.3435	1.76187	72.3231

The interference pattern when they arrive the sensor array (or screen) can be found by calculating the path difference between two adjacent slits.

$$n\lambda = d \sin\theta \tag{2.5}$$

where d d is the distance between two adjacent slits, θ is the angle of emeregence (analogous with the angle of deviation for the prism) and n is any positive integer.can be found using the grating constant *N*, which is the number of slits per unit length, where $d = 1/N$. Since the path difference between every slit is constant, waves leaving every slit will constructively interfere at the same location, which will be dependent on the wavelength of the incident wave. Similarly, there will also be destructive interference satisfying the below equation

$$n\frac{\lambda}{2} = d \sin\theta \tag{2.6}$$

Figure 2.2 shows the working principle of a diffraction grating. Multiple light interferences occur for different path lengths that are integer multiples of the wavelength and multiple dark interferences occur for path length that are integer multiples of half the wavelength.

This pattern of light and dark areas are called a fringe pattern. Any single wavelength incident to the grating will create a fringe pattern that depends on the wavelength and the grating topology.

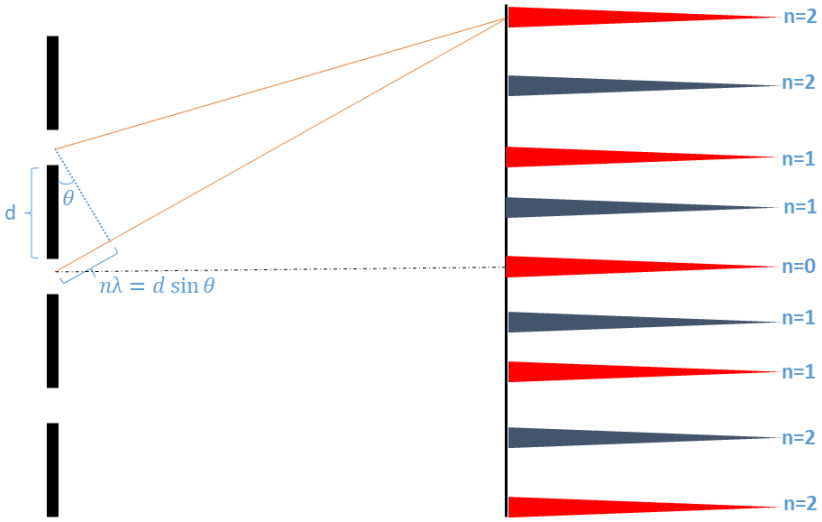

Figure 2.2: Working principle of a diffraction grating

The location of a constructive interference on the sensor array can be found by using:

$$y_n = \frac{n\lambda L}{d} \tag{2.7}$$

where L is the distance between the grating and the sensor array. From this equation it can be seen that the resolution of the grating spectrometer depends on the distance between the slits and the distance between the sensor array and the grating. Although the amount of increase for L is limited, d can be made adequately small achieving high-resolution [17], the main limitation of the grating spectrometer is due to multiple fringe patterns overlapping as the amount of wavelength components in the input light increases. Since each wavelength will create fringe patterns, these patterns will overlap and saturate the sensor array, resulting in a limted spectral range for the grating based spectrometers. Even though it is possible to bypass this issue with some additional propagation methods[18], these often increase the complexity of the design and hence the cost too.

2.3 Speckle Spectrometers

Speckle patterns are intensity patterns generated by interference of wave fronts having the same frequency but differing phases and amplitudes [19]. This results in a wave whose intensity varies randomly throughout the propagation path. The generation of

speckle patterns are mainly due to scattering of waves, where each scattered wave front can be modeled as a random angled vector in space.

An electromagnetic wave is coherent when it is made up of waves of same frequency, same waveform and a constant phase difference. When a coherent wave, e.g. a laser beam, interacts with a surface, each point the scattered wave front acts as a source of secondary spherical waves as stated in Huygens-Fresnel principle. If the roughness of the surface is enough to create optical path-length differences larger than one wavelength, a phase changes greater then 2π occurs. This creates a varying phase difference and thus making the light incoherent. The incoherence then results in interference of wave fronts, resulting in a randomly varying intensity pattern [20]. Low coherent light on the other hand generally do not produce speckle patterns, due to speckle patterns of different wavelengths averaging each other out.

The main form of scattering that generates the varying phase difference is elastic scattering as it conserves the kinetic energy of the scattering light but modifies the direction of propagation. In this process, the wavelength of the incident wave plays an important role as the particle size in relation to the wavelength determines the way electromagnetic waves scatter. For example, Mie scattering occurs when particle diameter is similar to or larger than the wavelength of the incident electromagnetic wave and its intensity depends on the angle of incidence of the incident wave [21].

An example of scattering based speckle patterns used in spectroscopy is presented in [22], where an on-chip random structure scatters the input signal and creates wavelength dependent speckle pattern, achieving 750 pm resolution. Another method of speckle generation used in speckle spectrometry is using multimode fiber optic cables. Light entering a multimode fiber optic cable propagates through different modes of the fiber, which have differing pathways inside the fiber optic cable. This difference in propagated paths creates a varying phase difference between the modes hence creating a speckle pattern at the exit of the fiber optic cable. In this speckle spectrometer architecture the length of the fiber optic cable greatly affects the resolution of the spectrometer, as increased cable length results in better resolution, achieving resolution in tens of picometers [8]. The working principle of speckle spectrometers is built upon the fact that the speckle patterns act as a fingerprint, uniquely identifying the wavelength of the input signal and the systems response to that signal. This being the case, the wavelength-dependent speckle patterns are first

measured and stored in what is called the calibration stage and later used to reconstruct the input spectrum the stored patterns [8, 10]. The resolution of a speckle spectrometer depends on how rapidly the speckle patterns decorrelate with respect to wavelength change, also called the spectral correlation width.

3. SPECKLE ENHANCED PRISM SPECTROMETER (SEPS)

3.1 Working Principle

The introduction of scattering induced speckle patterns to a prism spectrometer aims to combine the superioir resolution of the speckle pattern based spectrometers with high free spectral range of prism spectrometers. The scattering is achieved by placing a scattering medium in the propagation path of the light. The scattering medium is thick enough to allow multiple scattering instances to occur, this way effectively increasing the optical path length, which scales as l_t/L^2, where l_t is the mean free path and L path length [22, 25].

This scaling results in increased wavelength dependency of the speckle pattern due to l_t staying constant while L varies quadratically, enhancing the decorrelation of the speckle patterns with respect to wavelength change. In other words, speckle correlation scales inversely with l_t/L^2 too. As the scattering gets stronger the l_t value will get smaller, leading too a smaller speckle correlation width hence a better spectral resolution.

The $1/L^2$ scaling also allows a high resolution to be implemented in a small footprint. However, since the transmission through the scattering medium is approximately l_t/L, most of the input signal is not transmitted as L gets much larger than l_t, resulting in a decreased spectrometer efficiency [20-22].

Generally, a prism spectrometer maps the spectrum in a 1D manner and changing the wavelength displaces the location of the strip of light in the left portion of Figure 3.1 in the x-axis, moving it to left or right. Speckle patterns generated with a scattering medium alone, on the other hand, creates a 2D spectral-to-spatial mapping. Changing the wavelength alters the generated speckle pattern without displacing the location of the pattern on the x-axis. This being the case, as the wavelength interval increases the created speckle patterns corresponding to different wavelength components overlap and decrease the speckle contrast, in turn decreasing the efficiency of the spectrometer.

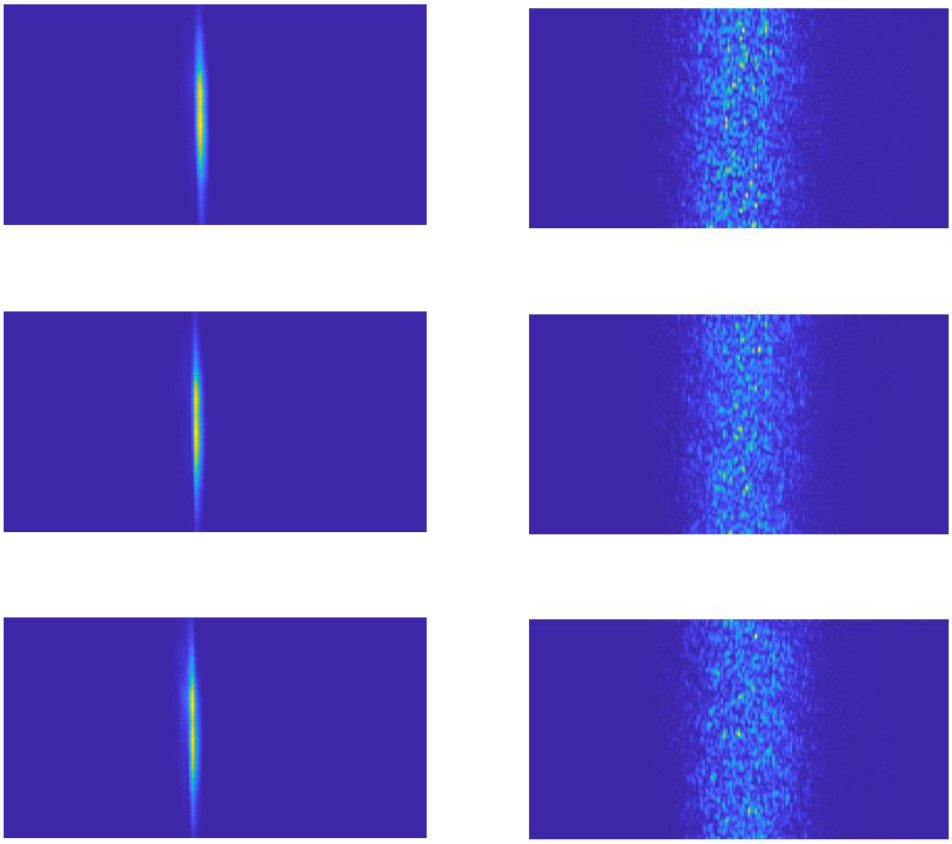

Figure 3.1: Prism and speckle pattern change with $\Delta\lambda$=1 nm

In SEPS, integrating the scattering medium to a prism spectrometer enables the mapping of different wavelength components to different speckle patterns and different locations on the detector array. Thus, an enhanced 2D spectral-to-spatial mapping is achieved by combining the prism with a scattering medium. This way SEPS exploits the high-resolution aspect of the speckle patterns with high spectral range aspect of a prism spectrometer.

The dynamic range of the spectrometer can be defined as the range of wavelengths the device can distinctly differentiate and measure, i.e. the wavelength range to resolution ratio, which can be defined as

$$Dynamic\ Range = \frac{\Delta\Lambda}{\Delta\lambda} \tag{3.1}$$

where $\Delta\Lambda$ is the continuous wavelength range and $\Delta\lambda$ is the device resolution. $\Delta\Lambda$ mostly depends on the detector used and since a CCD camera (ThorLabs 1.4

Megapixel Monochrome Scientific Camera) was used in this work, the effective wavelength range depends on the sensor width of the camera, which is 8.98 mm.

To calculate the resolution of the prism in the absence of a scattering medium, the FWHM of the strip of light is measured. Theoretically [24]:

$$\Delta\lambda_{prism} = \frac{4 \ln 2 \lambda}{\delta' W 2\pi} \tag{3.2}$$

where δ' is the angular dispersion (angle of deviation), W is the FWHM of the collimated beam arriving at the prism, and λ is the wavelength of the beam. The measured beam width is W=5 mm and the used wavelength is λ=855 nm. Plugging in the values in Equation 2.4, we get δ'=0.504x10^{-4} rad/nm, from this the theoretical resolution of the prism is $\Delta\lambda_{prism} \cong$1.488 nm. Taking the prism alone dynamic range as the device base dynamic range, DR_{prism} we can quantify the dynamic range enhancement as:

$$DR_{SEPS} = KDR_{prism} \tag{3.3}$$

where K is the gain factor due to the speckle patterns and is proportional degree of scattering introduced into the system by the scattering medium. The resolution gain factor can also be expressed as:

$$\Delta\lambda_{SEPS} = \frac{\Delta\lambda_{prism}}{K} \tag{3.4}$$

The resolution of the SEPS device – with any selected scattering medium – is found by calculating the correlation between the speckle patterns of consecutive wavelengths. For this, a speckle correlation function is utilized [8]:

$$C(\Delta\lambda, x) = \frac{\langle I(\lambda, x) I(\lambda + \Delta\lambda, x) \rangle}{\langle I(\lambda, x) \rangle \langle I(\lambda + \Delta\lambda, x) \rangle} - 1 \tag{3.5}$$

where $I(\lambda, x)$ denotes the intensity recorded at certain wavelength (λ) and position (x), $\Delta\lambda$ refers to the wavelength difference among speckle patterns for which the correlation is calculated and $\langle . \rangle$ is the mean operation. The correlation function calculates the amount of decorrelation each spatial location (pixel) in the speckle pattern. Figure 3.2 shows a visual interpretation of the correlation function. The yellow arrows represent the change of spatial independent variable x and the red arrows show the spectral independent variable $\Delta\lambda$ of the correlation function. Although it is possible to calculate the exact speckle pattern captured by the CCD camera generated by each

wavelength component λ_i, this requires the precise knowledge of the volumetric distribution of the scattering medium and the spatial profile of the input signal, which is not practical for a real world application. Instead, an experimental calibration process is used similar to [8].

The correlation function is calculated for each λ_i in the calibration sequence, resulting in a correlation curve, which can be seen in Figure 3.3.

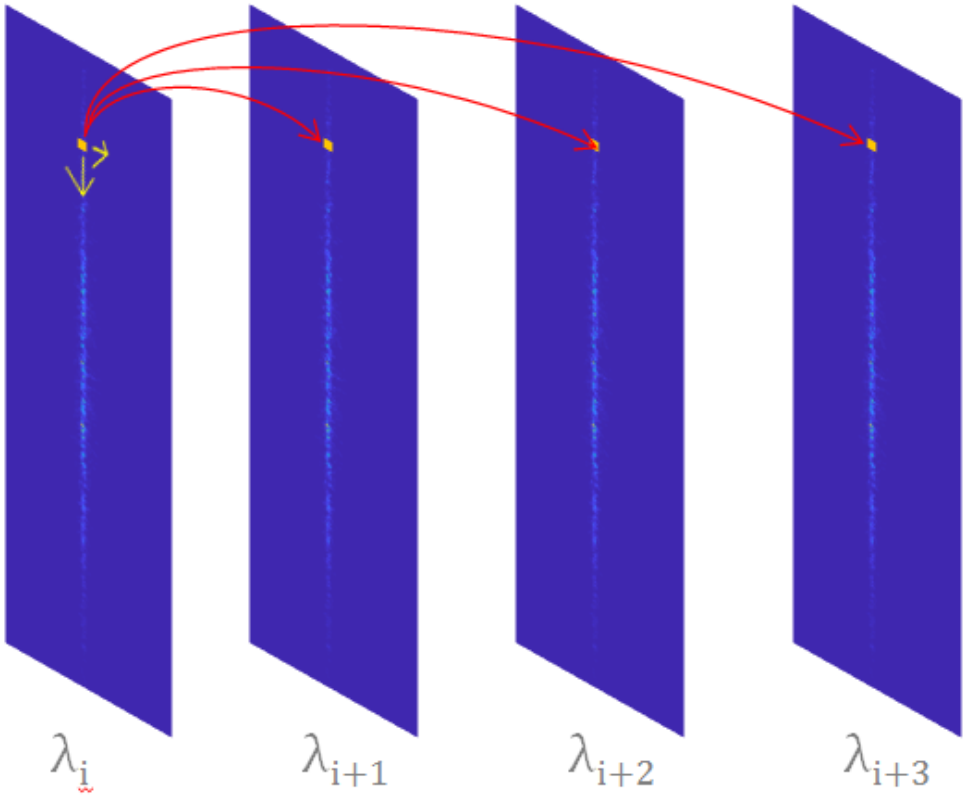

Figure 3.2: Visual representation of the correlation function

The resolution of the device is acquired by:

$$\Delta\lambda_{SEPS} = \frac{C(\lambda_0)}{2} \tag{3.6}$$

where λ_0 is the first wavelength step the calibration sequence. The device resolution is the HWHM of the correlation function curve. The achieved resolution gives the closest adjacent wavelengths that can be reconstructed by SEPS.

The spectrum output of the spectrometer is achieved by a reconstruction process, which uses the wavelength dependent speckle patterns gathered during the calibration

phase. The intensity distribution $I(\boldsymbol{r})$ of a given speckle pattern, where $\boldsymbol{r}$ is a spatial vector can be found as:

$$I(\boldsymbol{r}) = \int S(\lambda)X(\boldsymbol{r},\lambda)A(\lambda)d\lambda \tag{3.7}$$

where $S(\lambda)$ is the spectal flux density of the input signal, $X(r,\lambda)$ is the position dependent transmission function of the sacttering medium and $A(\lambda)$ is the spectral sensitivity of the camera. Since it is not practical to measure the spectral response of

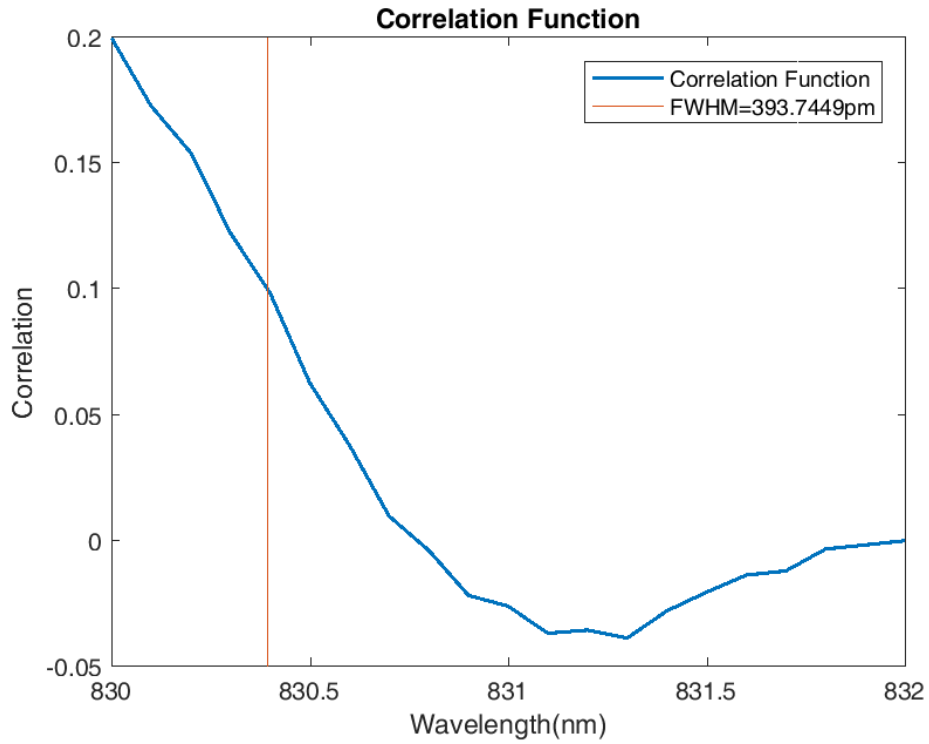

Figure 3.3: Correlation curve for a TiO_2 scatterer with concentration 1:75 and thickness 125µm. The orange line represents the HWHM.

the scattering medium and the camera separately, a transmission function of the whole system is defined:

$$T(\boldsymbol{r},\lambda) = X(\boldsymbol{r},\lambda)A(\lambda) \tag{3.8}$$

$T(\boldsymbol{r},\lambda)$ characterizes the spectral-to-spatial mapping of the whole SEPS system and Equation 4.7 then becomes:

$$I(\boldsymbol{r}) = \int S(\lambda)\,T(\boldsymbol{r},\lambda)d\lambda \tag{3.7}$$

The above equation can be discretized since in practice the spectral channels are spaced by $d\lambda$. The spatial channels can also be discretized since the camera sensor array consist of discrete pixels. Thus, Equation 3.7 becomes:

$$I = T \cdot S \tag{3.8}$$

The discretized matrices have the following structure:

$$\begin{bmatrix} I_1 \\ \vdots \\ I_n \end{bmatrix} = \begin{bmatrix} I_1^1 & \cdots & I_1^m \\ \vdots & \ddots & \vdots \\ I_n^1 & \cdots & I_n^m \end{bmatrix} \begin{bmatrix} \lambda_1 \\ \vdots \\ \lambda_m \end{bmatrix} \tag{3.9}$$

There are n spatial channels in the camera intensity vector I, and m spectral channels in the spectral flux vector S. Transmission matrix T has m columns each corresponding to a calibration image with n spatial channels.

Since the intended application of a spectrometer device is to find the input spectra, Equation 3.8 is modified to acquire:

$$S = T^{-1}I \tag{3.10}$$

This operation is the basis of the reconstruction process of the SEPS device and will be investigated further in Section 3.6.

3.2 Experimental Setup

The SEPS architecture consists of three main stages; the scattering stage, the prism stage and the image acquisition stage. The scattering stage focuses the light on the scattering medium using a cylindrical lens. The use of cylindrical lenses allow focusing on a single direction, creating a focused line on the scattering medium. The usage of the cylindrical lens is crucial at this stage to ensure adequate light-scattering particle interaction occurs. If a circular lens is used, the point focusing on the scatterer greatly reduces the amount of scattering and thus decreases the speckle area on the camera.

Light exitting the scattering medium then passes through a 50 um slit used to limit the spread of diffused light parallel to the focusing direction, this way effectively increasing the dynamic range of the SEPS device. The light exiting the slit is then incident on another cylindrical lens used to collimate the light beam.

The prism stage ensures the speckle patterns generated does not overlap and decrease the speckle contrast on the camera.

The image acquisition stage consists of mirrors and another cylindrical lens. The cylindrical lens focuses the collimated beam onto the CCD camera.

Figure 3.4 and 3.5 show the simplified and the actual experimental setup and Table 3.1 shows the corresponding components in the setup, which are also marked with numbers in Figure 3.5. Figure 3.5 also depicts the three stages of the system with rectangles.

3.3 Scattering Medium Preparation

Multiple scattering mediums were tried to find an optimal scatterer, which provided a high resolution without drastically reducing the transmitted power. First approach was to use easily obtainable household items such as sketching paper, adhesive tape and parchment.

Further scatterer preparation was done to better control the resolution gain and transmissivity of the scattering medium. The scatterer's were prepared using TiO_2 (Titanium Dioxide) nanoparticles and Norland Optical Adhesive epoxy. The nanoparticles were suspended in the epoxy in different concentration and width combinations. The preparation process can be seen in Figure 3.6 in detail. The first step in scatterer preparation is to measure and mix the two components (Figure 3.6a), followed by dripping the mixture in between two glass slides (Figure 3.6b). The glass slides are set apart before the dripping is done and the used thicknesses for the scatterers are 125 μm, 250 μm, 400 μm and 750 μm. The dripping process ensures that the thickness of the scattering medium is uniform. Finally the prepared slides are cured under a UV light (Figure 3.6c). The duration of the curing process is proportional to the TiO_2 : Epoxy ratio. The used concentration values are 1:5, 1:12, 1:25, 1:50 and 1:75. These scattering mediums were combined with a 50 um slit and placed in between two class slides for structural stability, as can be seen in Figure 3.6b.

Although the preparation process ensures a uniform thickness, the distribution of TiO_2 particles is not necessarily homogeneous and this due to the viscous nature of the mixture. Even though the curing step was done while holding the slides in a horizontal position, the flow of mixture in between the glass slides was not controlled. However,

this heterogeneity did not affect the operation of the spectrometer device, as the calibration of the system implicitly included the effects of scatterer heterogeneity.

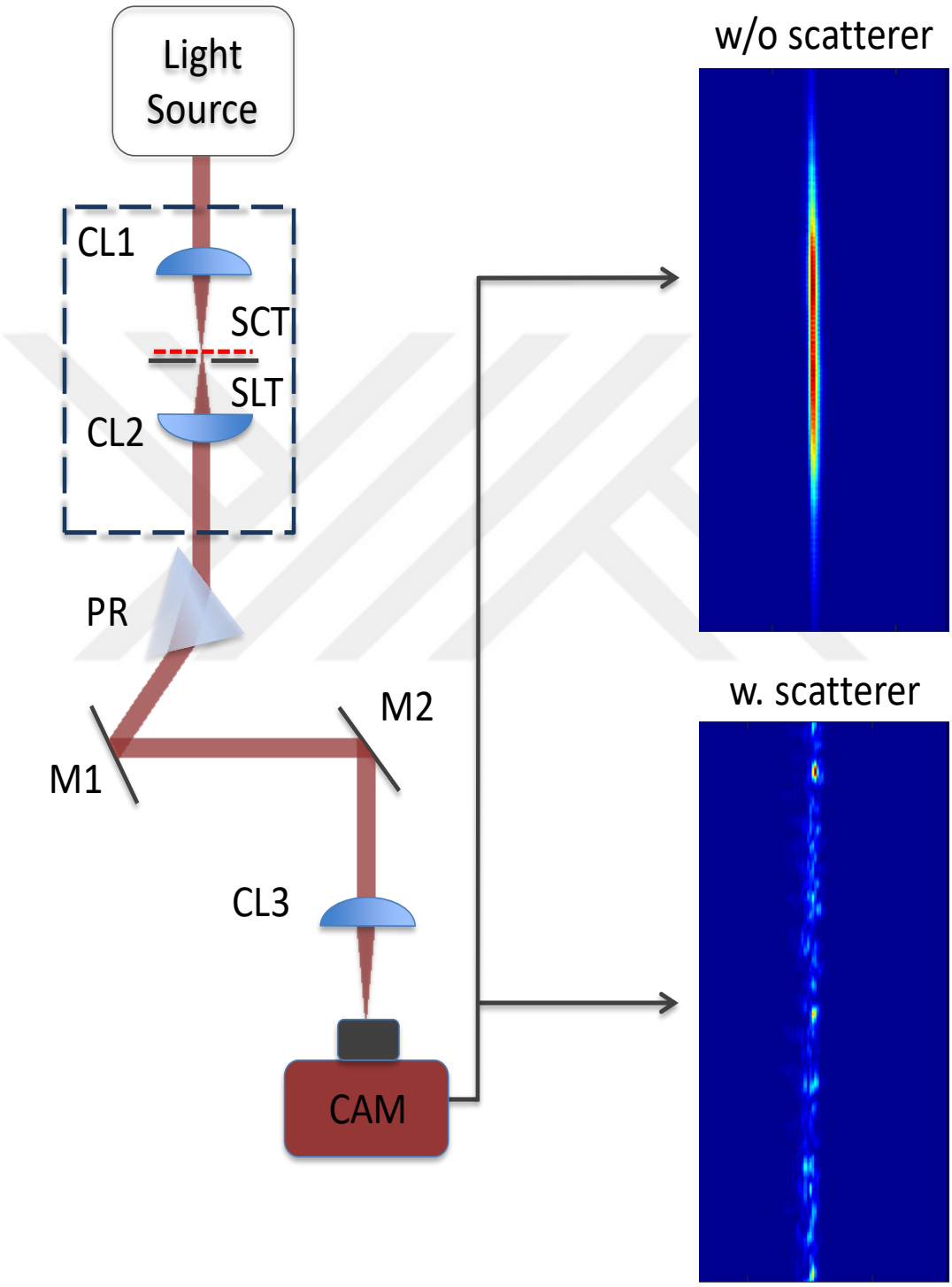

Figure 3.4: Simplified experimental setup

Table 3.1: Corresponding setup components

Part	Part No	Name	Description
Light Source	1	Tunable Laser/SLD	Input light source to the system
	2	Collimator	Collimates the fiber output
CL1	3	Cylindrical Lens	Line focuses the incident light onto the scattering medium
SCT	4	Scattering Medium	The scattering medium and the slit are back to back on top of a translation stage.
SLT	4	Slit	
CL2	5	Cylindrical Lens	Recollimates the light before the prism stage
PR	6	Prism	Disperses the generated speckle pattern
M1,M2	7,8	Mirrors	
CL3	9	Cylindrical Lens	Line focuses the light onto the camera
CAM	10	Camera	Records the speckle pattern

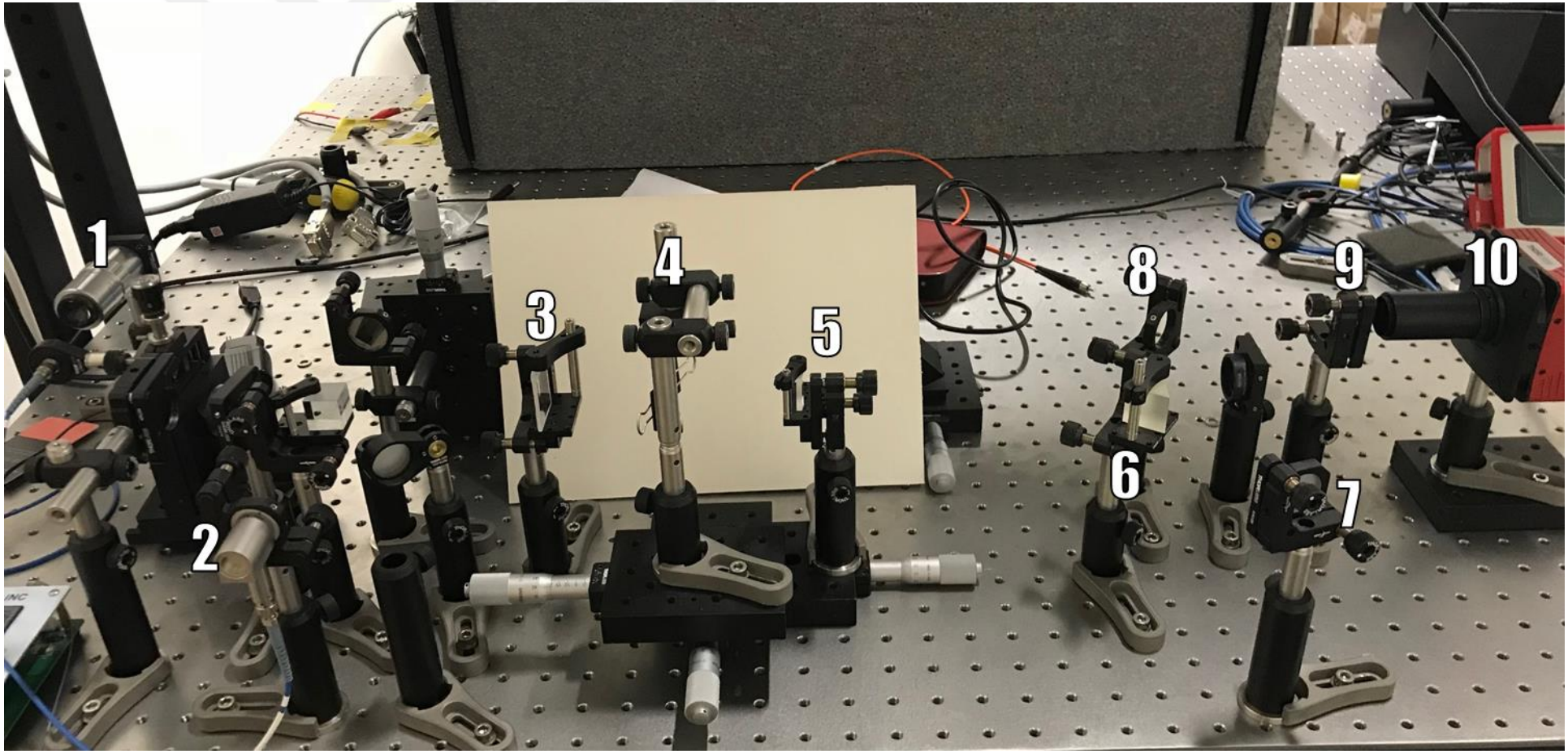

Figure 3.5: Experimental Setup

3.4 System Characterization

A series of experiments were done to characterize the SEPS device with the prepared scattering mediums. The main characteristics done were to measure the transmissivity and the resolution of the scattering medium.

Resolution calculation was done by taking calibration images with $d\lambda$=25 pm and $\Delta\lambda$=1.8 nm, which is an adequate interval that encompasses the prism resolution. Applying Equation 3.5 to 73 calibration images and calculating the HWHM, we get the system resolution for each scattering medium.

To measure the transmissivity, the total intensity on the camera was recorded with and without a scattering medium present. The system setup was unchanged during this process and the exposure settings of the camera was digitally accounted for furing calculations.

It should also be noted that characterization experiments were done without using the 50 um slit placed after the scattering medium. This was due to the scattering medium preparation process, resulting in thin scatterers to be deformed while separating from the glass slides. This, however, did not affect the characterization process since the presence of a slit equally reduces the transmissivity of each scattering medium.

The lack of a slit also increases the speckle pattern area, effectively reducing the dynamic range of the device, but since the spectral range constant at 1.8 nm, this too does not affect the results of the characterization experiments.

Table 3.2 show the transmission and resolution values of each scattering medium prepared with a TiO_2 epoxy mixture. The transmission values are percent values and the resolution values are all in picometers.

In addition, Figure 3.7 also depicts the change in transmission and resolution as the thickness and concentration of the scattering medium changes. The solid and dashed lines correspond to transmission and resolution values, respectively.

The increase in both the concentration and the thickness improve the resolution of the system, but at the same time decreases the light efficiency. It should also be noted that increasing the concentration, although improves the resolution in linear trend; the amount of transmission lost is not linear. The transmission of the scattering medium plateaus for concentration values larger than 1:25.

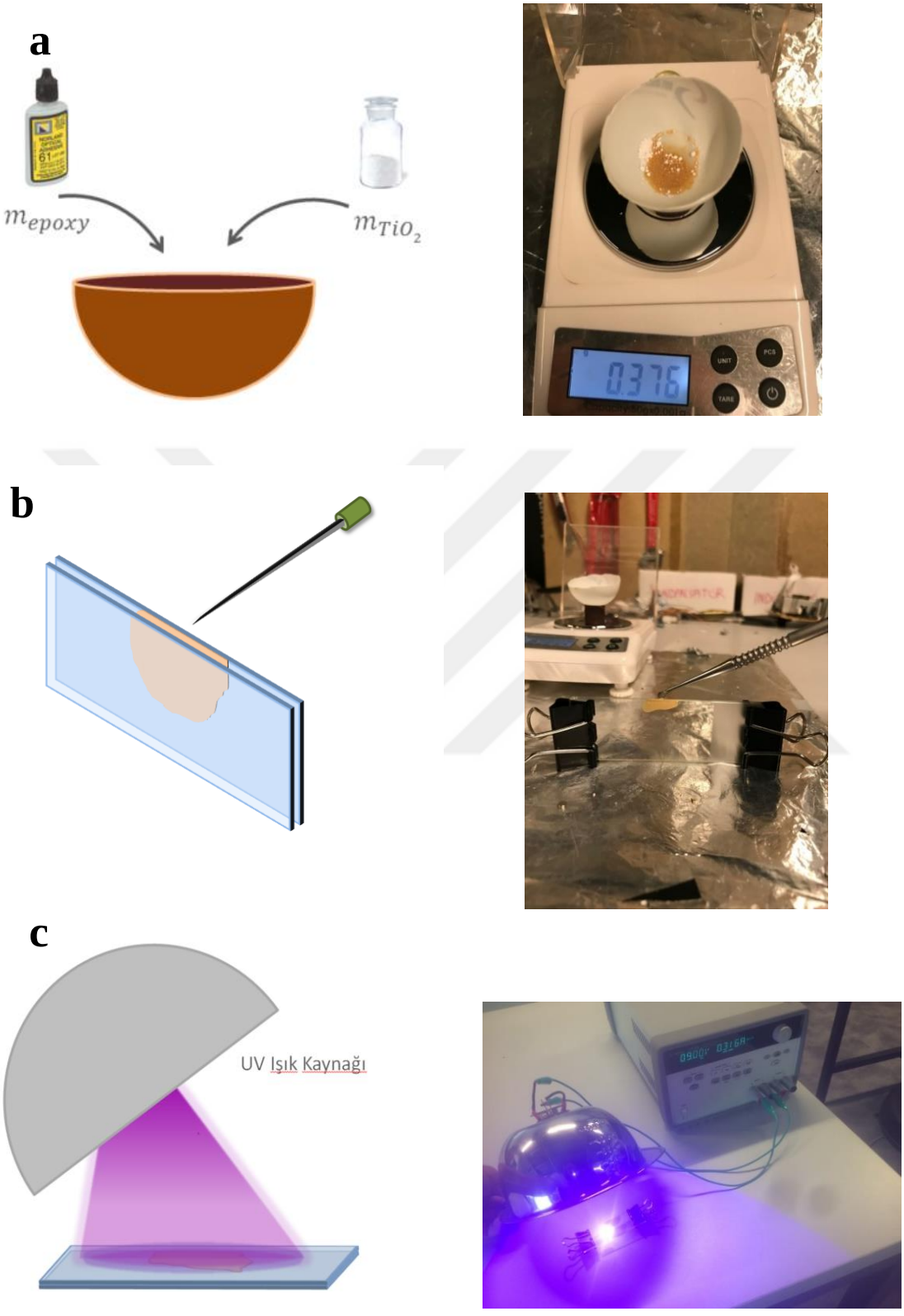

Figure 3.6: Preparation of scatterers

Table 3.2: Transmisson and resolution values for prepared scattering mediums

Thickness (μm)	Concentration	Resolution (pm)	Transmission (%)
125	1:5	152,91	0.0457
	1:12	228,77	0.0788
	1:25	209,14	0.0728
	1:50	333,63	0.4054
	1:75	352,46	0.5677
250	1:5	97,78	0.0276
	1:12	132,39	0.0454
	1:25	201,61	0.0676
	1:50	272,58	0.5974
	1:75	275,99	1.0552
500	1:5	65,21	0.0182
	1:12	143,37	0.0535
	1:25	250,89	0.0728
	1:50	347,45	0.4136
	1:75	276,55	0.4016
750	1:5	33,53	0.0122
	1:12	86,54	0.0337
	1:25	195,14	0.0579
	1:50	192,96	0.0586
	1:75	259,68	0.0724

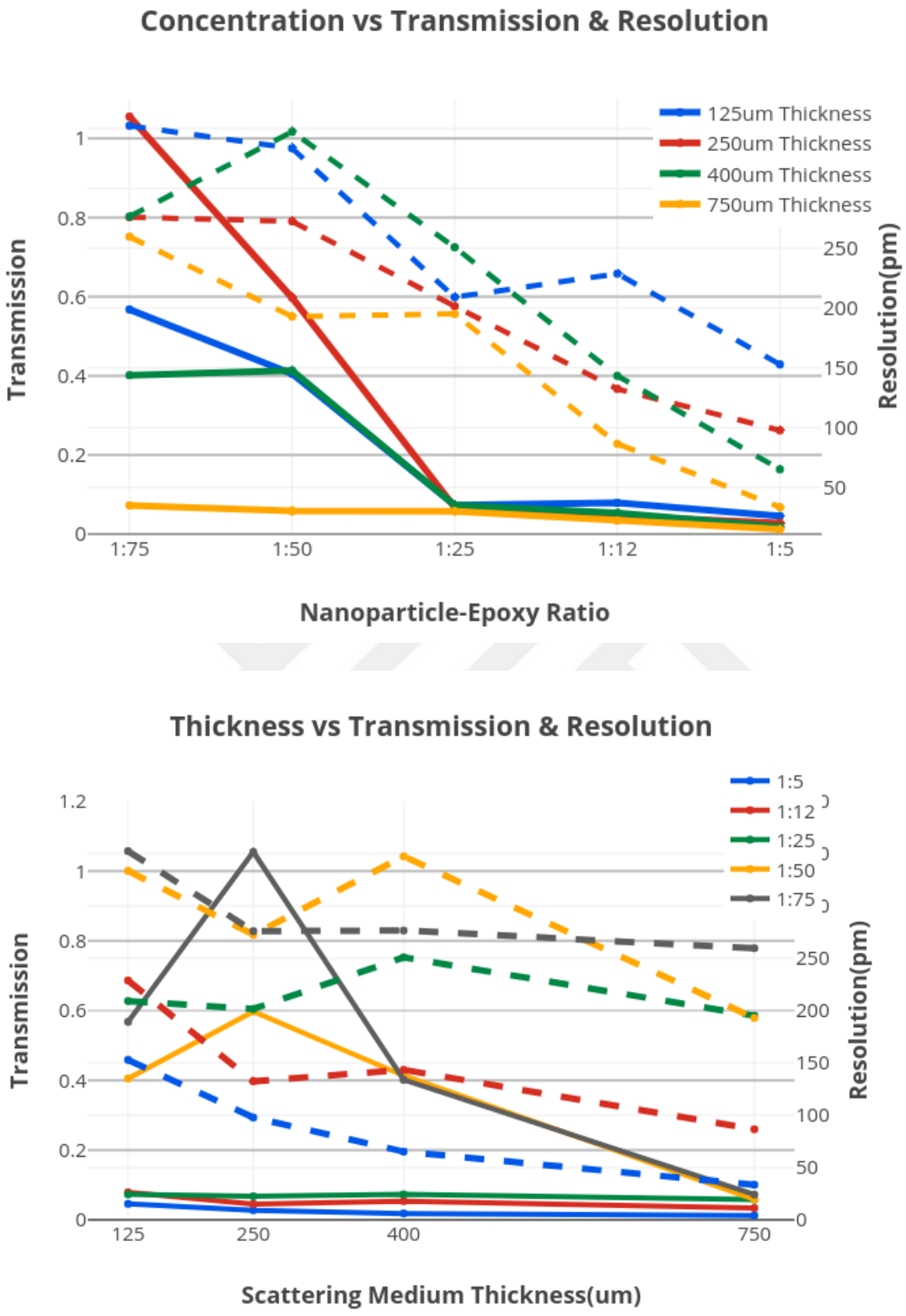

Figure 3.7: (a) Concentration vs Transmission & Resolution Graph and (b) Thickness vs Transmission & resolution Graph

For thickness values, the increase in thickness does not affect the resolution improvement as much as the concentration values, but greatly decreases the

transmission values for low concentration mixtures. From this we can conclude that to increase the resolution, increasing the concentration instead of scattering medium thickness will result in better resolution improvement.

The general relation between the transmission and resolution is plotted in Figure 3.8, where the blue dots represent the prepared scattering mediums and the orange line is the logarithmic fit line with $R^2 = 0.89$.

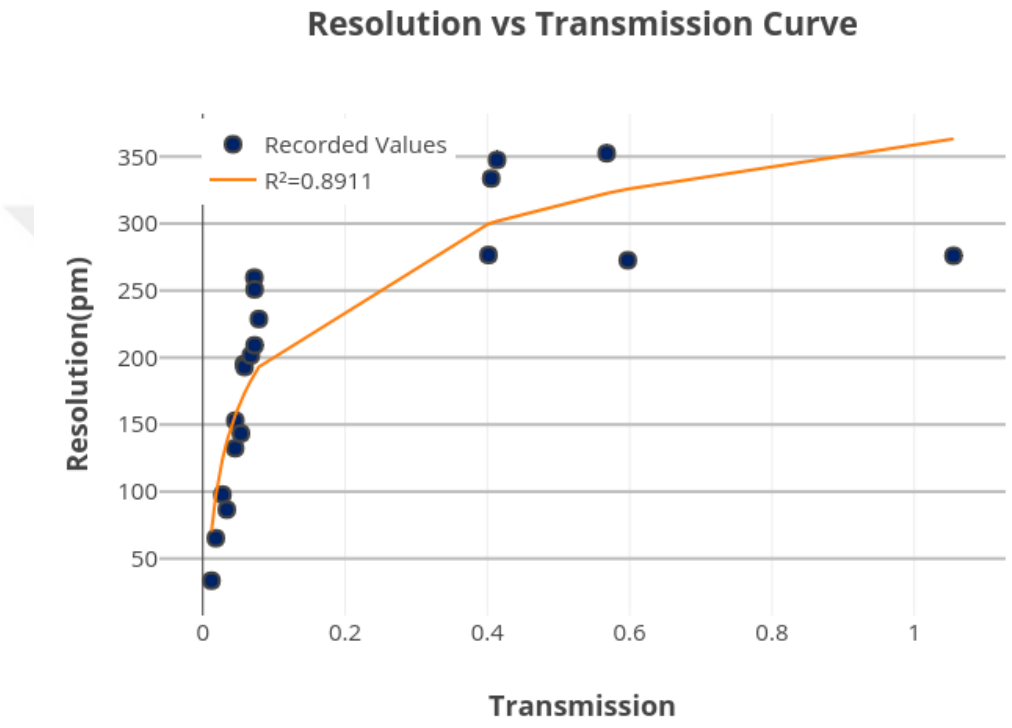

Figure 3.8: Transmission vs Resolution Curve

It can be concluded that the current topology of the system introduces a tradeoff between transmission and resolution. A thicker and more concentrated – with more TiO2 particles – scattering medium will increase the resolution drastically after a certain point, but since the transmission values at these parameters are around 0.1% the real world applications of this high resolution spectrometer will be limited. Various additions to the current topology will be discussed in Section 5.1 to alleviate this issue. It should be noted that although the resolution improvement seems unbounded, a practical limit is present on how the resolution can be enhanced using a scattering medium due to loss of transmission. This limit depends on the light power requirement of the application at hand, i.e. a SEPS device used in an OCT application that requires

10 mW of optical power delivered with an exposure time of 200 μs [25], has to satisfy a certain transmission ratio to work properly, effectively limiting the resolution gain.

3.5 Spectrometer Calibration

Calibration of the spectrometer, as was discussed in Section 4.1, requires recording a sequence of speckle patterns, with each image corresponding to a single λ value, ranging from λ_0 to $\lambda_0 + \Delta\Lambda$. Since, the used tunable laser source has the ability to sweep between 830 nm and 880 nm in 10 pm steps, the calibration sequence was chosen in between these ranges according to the desired reconstruction range.

The system can reconstruct any set of wavelength components as long as they are in the range without the need to calibrate for the whole range of the tunable laser; e.g. calibrating just for just between the range of 830 – 831 nm allowed the system to reconstruct any wavelength component in this range – and was resolvable by the system. In addition, wavelength steps used in calibration steps do not need to be uniformly seperated.

This was also beneficial since the calibration stage was time consuming due to a technical discrepancy between the tunable laser and the ThorLabs camere recording software. Figure 3.9 shows a set of calibration images with $\Delta\Lambda$= 400 pm and $\Delta\lambda$=10 pm, where the top left image is 854.8 nm and bottom right image is the 855.2 nm.

It can also be noted that since $\Delta\Lambda$ is considerably small compared to the prism resolution, the speckle patterns are stationary. As $\Delta\Lambda$ surpasses the prism resolution, the speckle patterns move too.

3.6 Spectrum Reconstruction

Section 3.1 briefly explains the underlying mechanism of spectrum reconstruion where a transmission matrix T is generated from the recorded calibration images and is used to reconstruct the input spectra I. This operation requires taking the inverse of the matix T. Directly taking the inverse of the matrix with Equation 3.10 gives the following reconstructed spectrum in Figure 3.10a. The reconstruction is done using the calibration images shown in Figure 3.9 to reconstruct a single wavelength, namely λ=855 nm.

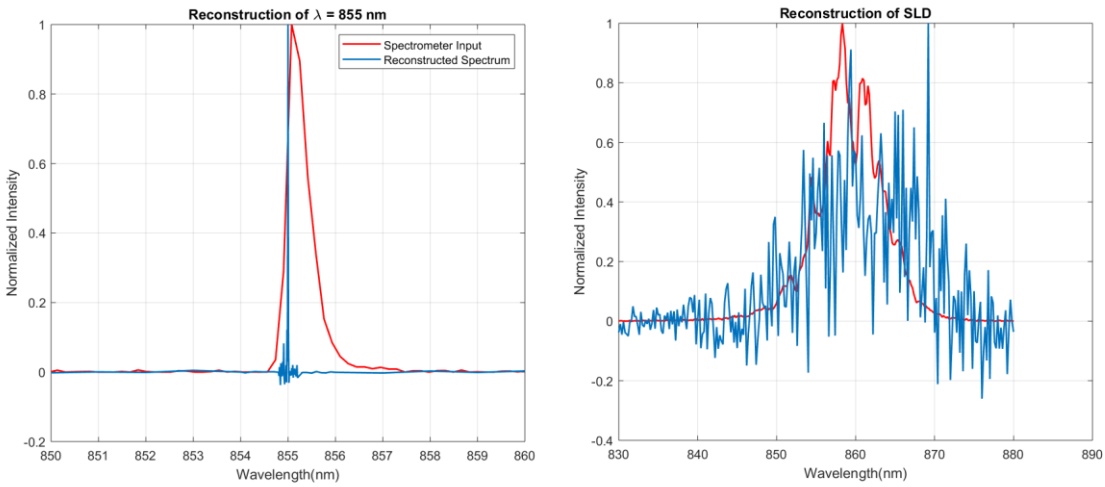

Figure 3.9: a) Reconstruction of a single wavelength input and b) reconstruction of a broadband input

The red plot shows the ThorLabs grating spectrometer based measurement and the blue plot is the reconstructed spectrum using Equation 3.10. It can be seen that the reconstruction works and and its resolution is better compared to a grating based spectrometer when used to reconstruct a narrowband input, but the performance greatly decreases as the input spectral range increases. Figure 3.10b is the reconstruction of a broadband source with the central wavelength λ_c=860 nm and FWHM = 10nm. There are several sources for experimental noise, mainly: (i) mechanical and thermal instability of the scattering medium, (ii) source switching, (iii) intensity fluctuation and wavelength drift of the tunable laser source and (iv) discrete intensity resolution of the CCD camera.

To understand the susceptibility of the reconstruction process we look at the condition number, κ, of T for the inversion operation,which measures how much the output can change with a small change in the input. In our case, how much the presence of noise will effect the reconstructed. As the condition number of T increases the matrix becomes "ill-conditioned" and thus the reconstructed spectrum will be greatly distorted due to experimental noise.

To calculate the condition number we can use the singular values in D, as the ratio of the largest and smallest values can give us the condition number of T. Looking at the condition numbers for both reconstructions in Figure 3.10 we get $\kappa(T)$=183 and $\kappa(T)$=81 for single peak and broadband inputs, respectively, meaning both are ill-conditioned and are highly prone to noise perturbations. Given these condition

numbers, it was expected for the SLD reconstruction to be better compared to single peak reconstruction although this wasn't the case. The reason for a larger "ill-condition" in the single peak case is due to the ratio of the speckle pattern to the rest of the used sensor area. Region is selected adaptively in calibration images during the image processing of the experimental data. Calibration for the SLD reconstruction requires a larger interval to be calibrated, specifically 251 calibration images with a step size of 200 pm, and this requires a smaller region to be selected compared to the single peak calibrations, which require a smaller interval to calibrate, hence a larger image region selection. Figure 3.11 compares the selected regions for both cases.

The discrepancy in condition number and the reconstruction result is due to source switching, which most probably leads to mechanical micro displacemenets on the system. On the other hand, the inputs for the single peak or multi peak reconstructions are acquired during the calibration phase by recording multiple images on a single calibration step and using one as a calibration image and the rest as input images. This minimizes the amount of noise that can distort the results.

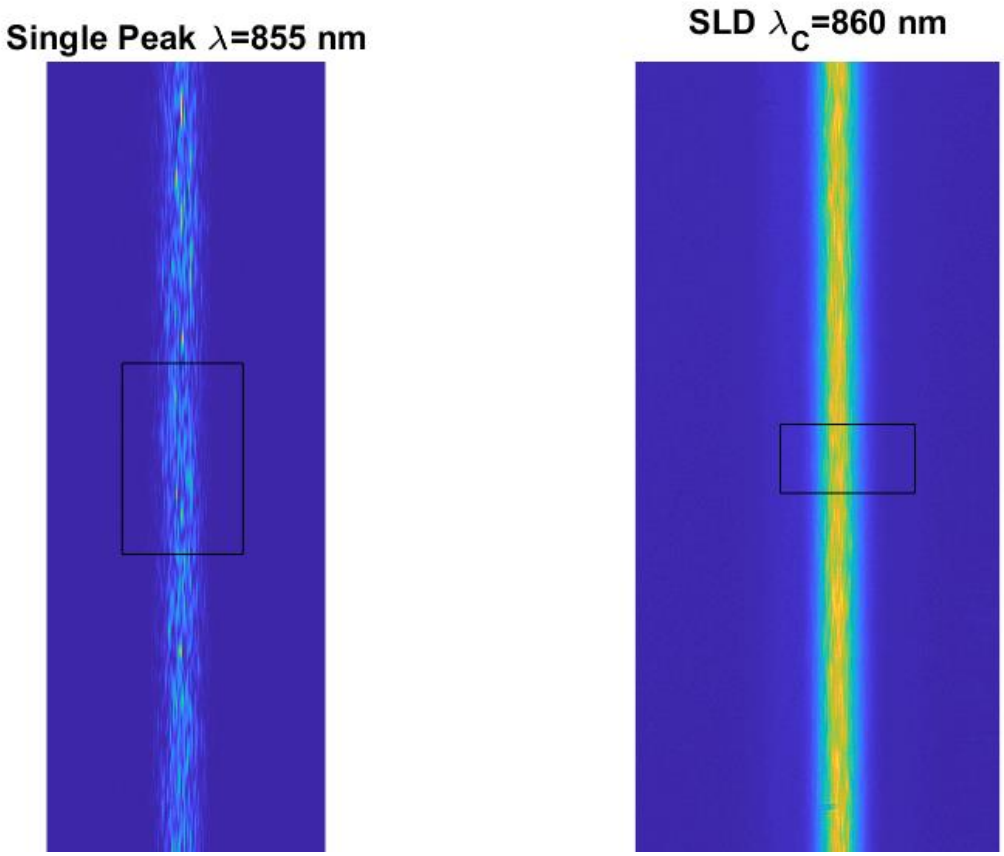

Figure 3.9: Region selections for single peak and SLD reconstructions

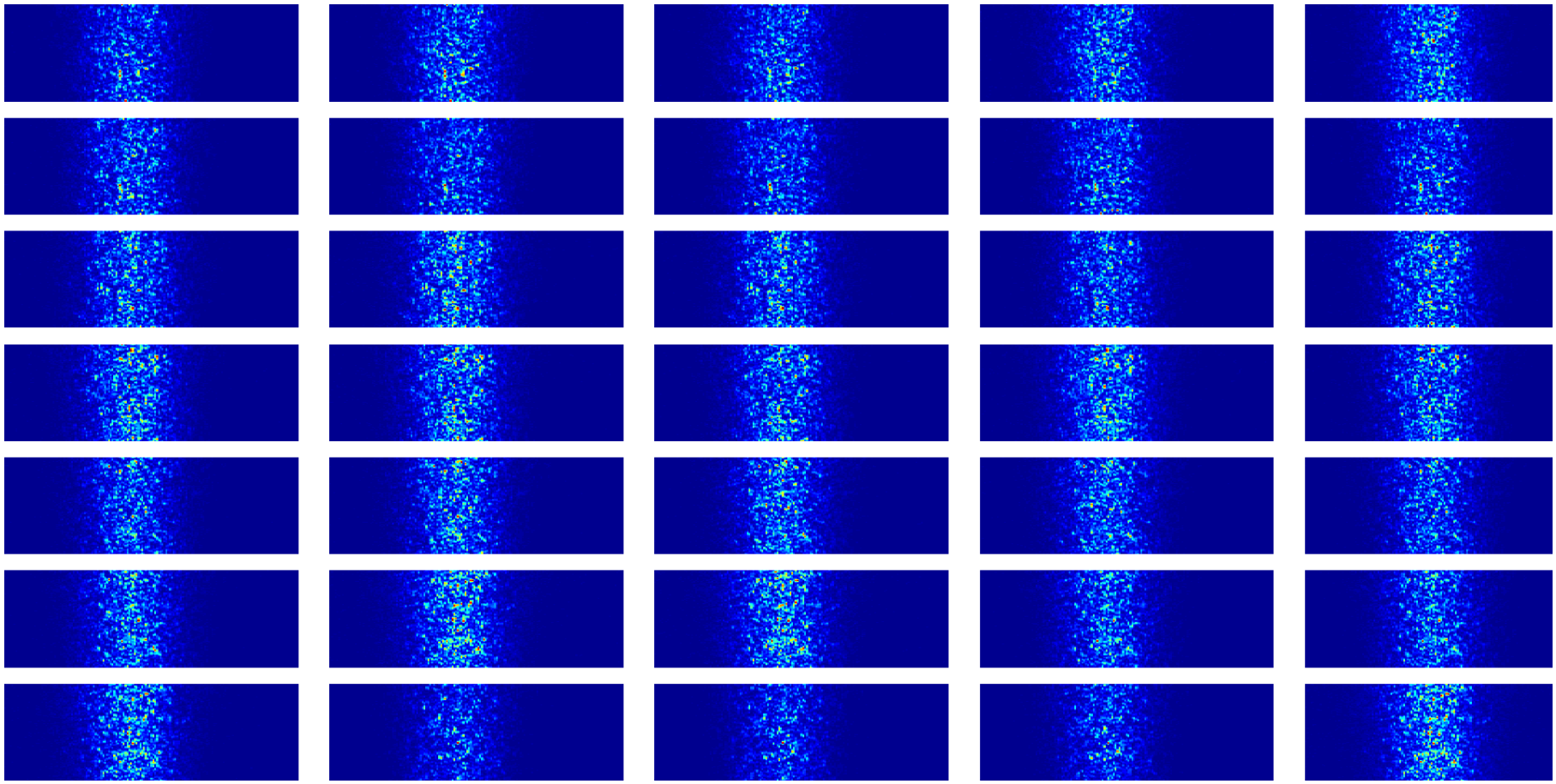

Figure 3.10: Calibration sequence with $\Delta\lambda$=10 pm and $\Delta\Lambda$=[854.80,855.20]

To bypass the effect of noise and improve the reconstruction performance a thresholding is applied. Since directly filtering the values of T will completely nullify the decorrelation calculation, it is necessary to apply filtering in a different fashion, mainly while taking the inverse of T. The pseudoinverse of the transmission matrix T is achieved by using the Moore-Penrose Inverse. Since the transmission matrix T consists of calibration images reshaped into $n \times 1$ column vectors where n corresponds to number of spatial channels (pixels), it is safe to assume that all the columns of the T is linearly independent and thus T is full rank. This allows the pseudo inverse to be written in the simple algebraic formula:

$$T^{+} = (T^{*}T)^{-1}T^{*} \tag{3.11}$$

Where $T^{+}$and T^{*} are the pseudoinverse and conjugate transpose of matrix T, respectively.

To apply thresholding we need to decompose T with singular value decomposition, $\boldsymbol{T = UDV^{T}}$, where U and V are $n \times n$ and $m \times m$ unitary matrices, respectively and D is an $n \times m$ diagonal matrix. Plugging in the decomposed T into Equation 3.11 we get[26]:

$$\begin{aligned} T^{+} &= (VDU^{T}UDV^{T})^{-1}VDU^{T} \\ &= (VD^{2}V^{T})^{-1}VDU^{T} \\ &= (V^{T})^{-1}D^{-2}V^{-1}VDU^{T} \\ &= VD^{-1}U^{T} \end{aligned} \tag{3.12}$$

Above conjugate transpose is replaced with transpose since every element in T is real valued. In addition, D is a diagonal matrix, which allows us to get D^{-1} simply by taking reciprocal of each value of D.

To find the optimal threshold, the effect of noise perturbation to the singular vectors is observed. If we assume a Gaussian noise with a standart deviation of σ_e, and write the perturbed matrix as

$$T_p = T + G \tag{3.13}$$

where G is the noise matrix, we can get the amount of distortion in j^{th}space by

$$T_p V_j = d_j U_j + G V_j \tag{3.14}$$

By taking the norms of elements on the right hand side, we can get the threshold for which noise perturbation is larger than the singular value. Since $\|d_j U_j\| = d_j$ and $\langle \|GV_j\| \rangle = \sigma_e \sqrt{m}$ where $\langle ... \rangle$ indicates averaging over all calibration steps, we can get the comparison value with wihich singular values can be discarded.

$$d_j < \sigma_e \sqrt{m} \tag{3.15}$$

This is because the amount of noise perturbation will suppress the transformation efect of the d_j value. To get the threshold this value is compared to the average largest singular value that can be estimated by $\langle d_1 \rangle = \tau \sqrt{nm}$ since T is composed of independent elements and τ is the mean speckle intensity. Finally we get

$$\langle d_1 \rangle threshold = \sigma_e \sqrt{m}$$

$$threshold = \frac{\sigma_e \sqrt{m}}{\tau \sqrt{nm}} \tag{3.16}$$

For the reconstruction in Figure 3.10b, calculating $\sigma_e = 7.3 \times 10^{-4}$ by using the multiple images taken during the calibration phase, and plugging in the rest of the values, we get $threshold = 0.0926$.

4. RESULTS

The performance of the proposed Speckle Enhanced Prism Spectrometer (SEPS) was first demonstrated through conducting a series of calibration routines and then recording the desired input spectrum to be reconstructed. Table 4.1 summarizes some of the tried scattering mediums

Table 4.1: Resolution, resolution gain and dynamic range of various scattering mediums

Scattering Type	Resolution (pm) ($\Delta\lambda_{SEPS}$)	Resolution Gain (K)	Dynamic Range (DR)
No scatterer	1680	1	450
Grinded glass	526	3.19	1,438
Adhesive tape	373.8	4.49	2,023
Sketch paper	201.7	8.32	3,750
Parchment	200.2	8.39	3,778
TiO_2 mixture 1	39.4	42.63	19,200
TiO_2 mixture 2	30	56	25,217
TiO_2 mixture 3	17.1	98.24	44,240

Experimentally, the amount of shift introduced by the prism is found to be 0.5434 px/nm, meaning that the light strip created by the prism shifted 0.5434 pixels for every 1 nm shift in the wavelength. Since the CCD sensor array has 1392 pixels in the horizontal direction the wavelength range is found to be $\Delta\Lambda$=756.4128 nm. In addition the experimental prism resolution was found to be 1.68 nm, leading to a dynamic range of 450. Similarly other scattering medium values were measured and calculated and a gain factor was calculated, quantifying the resolution enhancement the tested scattering medium introduced to the system. Plotting the correlation functions for these scattering mediums, we get Figure 4.1.

Note that the curves get steeper as the resolution improves, meaning that the speckle patterns rapidly decorrelate with wavelength change. The steepest curve, TiO2

mixture 3, is 750 µm thick and has a concentration of 1:120, achieving a resolution of 17.1 pm.

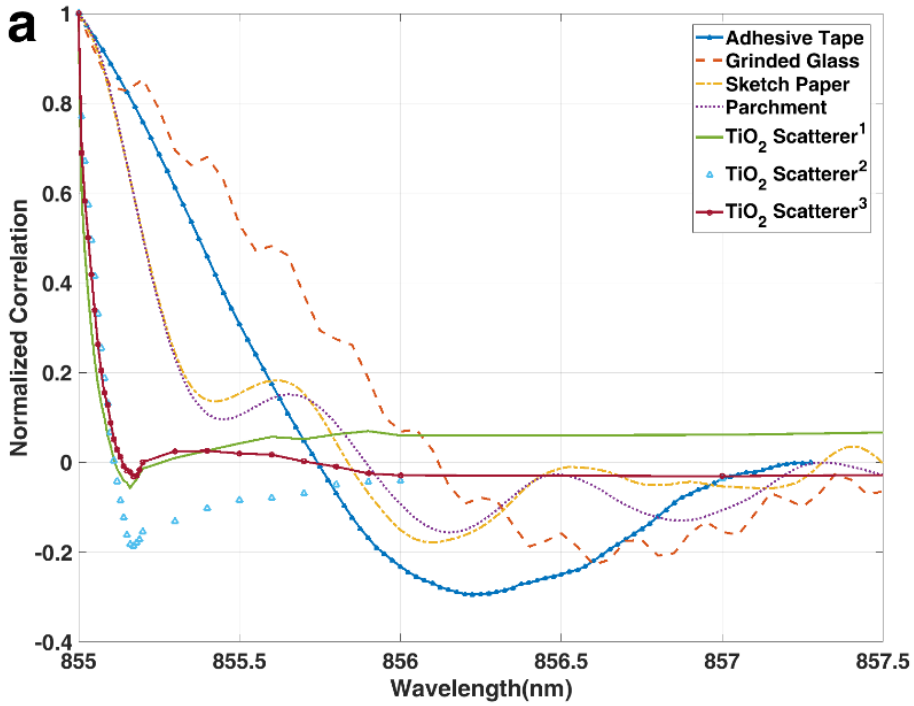

Figure 4.1: Correlation functions for various scattering mediums

The red line is again the output of a ThorLabs grating based spectrometer. As it can be seen from the above Figure, ThorLabs spectroemeter was unable to resolve the two peaks in each case, meanwhile SEPS was. Since the calculated resolution was 17.1 pm, the SEPS device was able to resolve 30 pm and was able to partially resolve the 20 pm input. 10 pm input, on the other hand, was unresolved for both spectrometers, which was the expected outcome.

The reconstruction of unfiltered and filtered SLD with a bandpass filter with λ_c=860 nm and FWHM = 10 nm with their corresponding optimal thresholds can be seen in Figure 4.4.

Calculating the correlation function from both sides of the central wavelength, we can get a wavelength profile of the correlation function. Figure 4.3 plots both the correlation function and the reconstructed spectrum of a single wavelength.

It can be seen from the figure that for both reconstructions the reconstruction values in higher wavelength steps are skewed and deviate from their actual values. This is

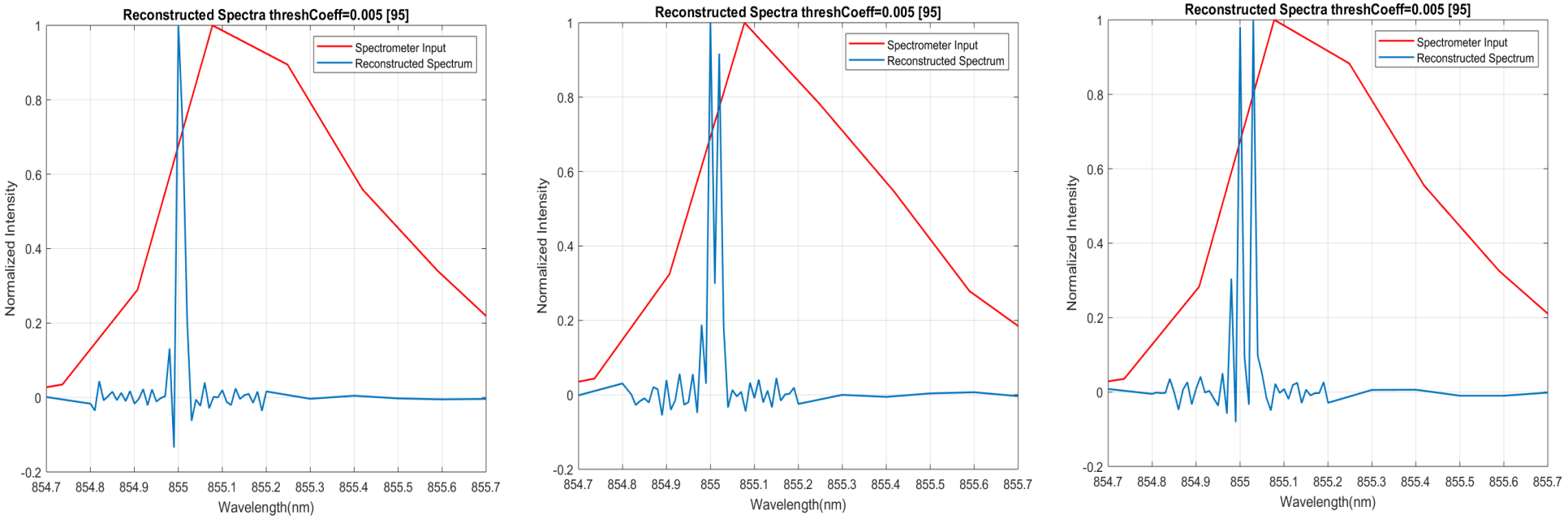

Figure 4.2: Reconstruction of different double peak inputs namely a) $\Delta\lambda$=10 pm b) $\Delta\lambda$=20 pm c) $\Delta\lambda$=30 pm

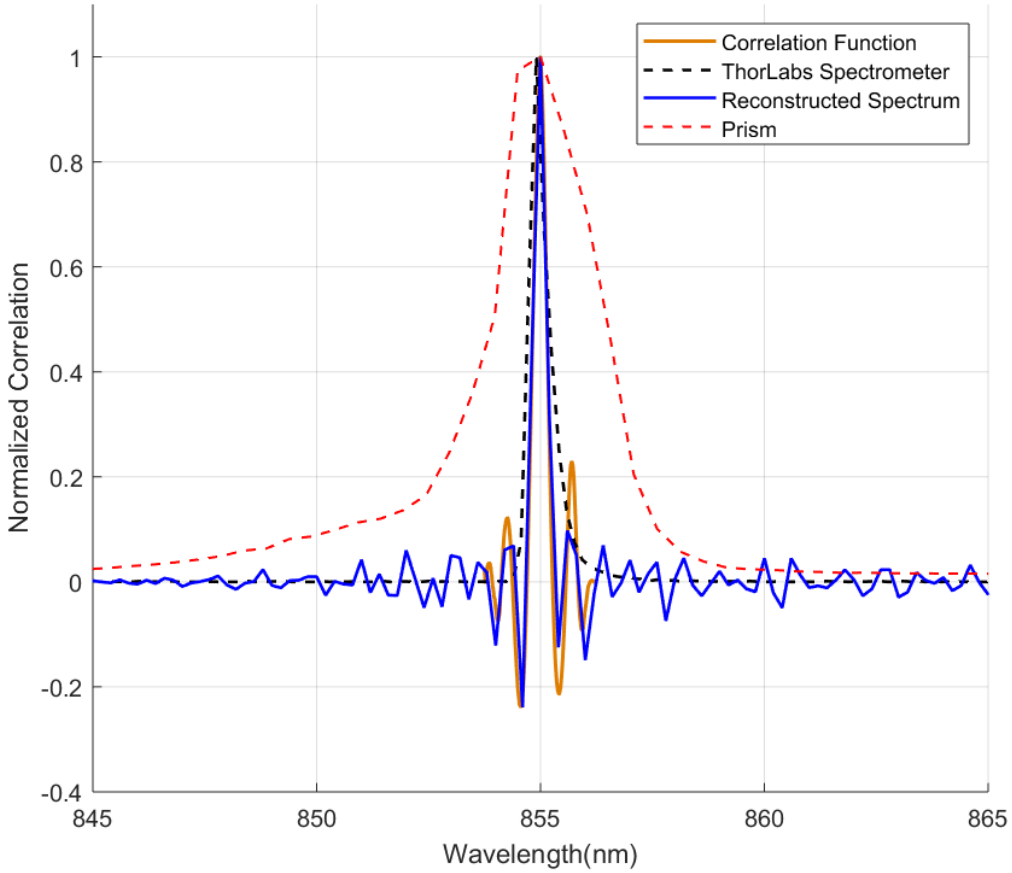

Figure 4.3: Correlation function and the reconstructed spectrum compared to prism and grating spectrometer

mainly because the wavelength precision and delivered power of the tunable laser decreases as it reaches its higher wavelength range limits. This decreases the speckle pattern contrast and thus further increases the effect of noise perturbation in those intervals. It should be added that since the tunable laser used in this work ranges from 830 nm to 880 nm, the wavelength range of the designed SEPS system was limited in these values. But using a tunable laser source with a higher wavelength range will increase the free spectral range of the system. It should also be noted that another drawback imposed by tunable laser source was the $\Delta\lambda$=10 pm step limitation.

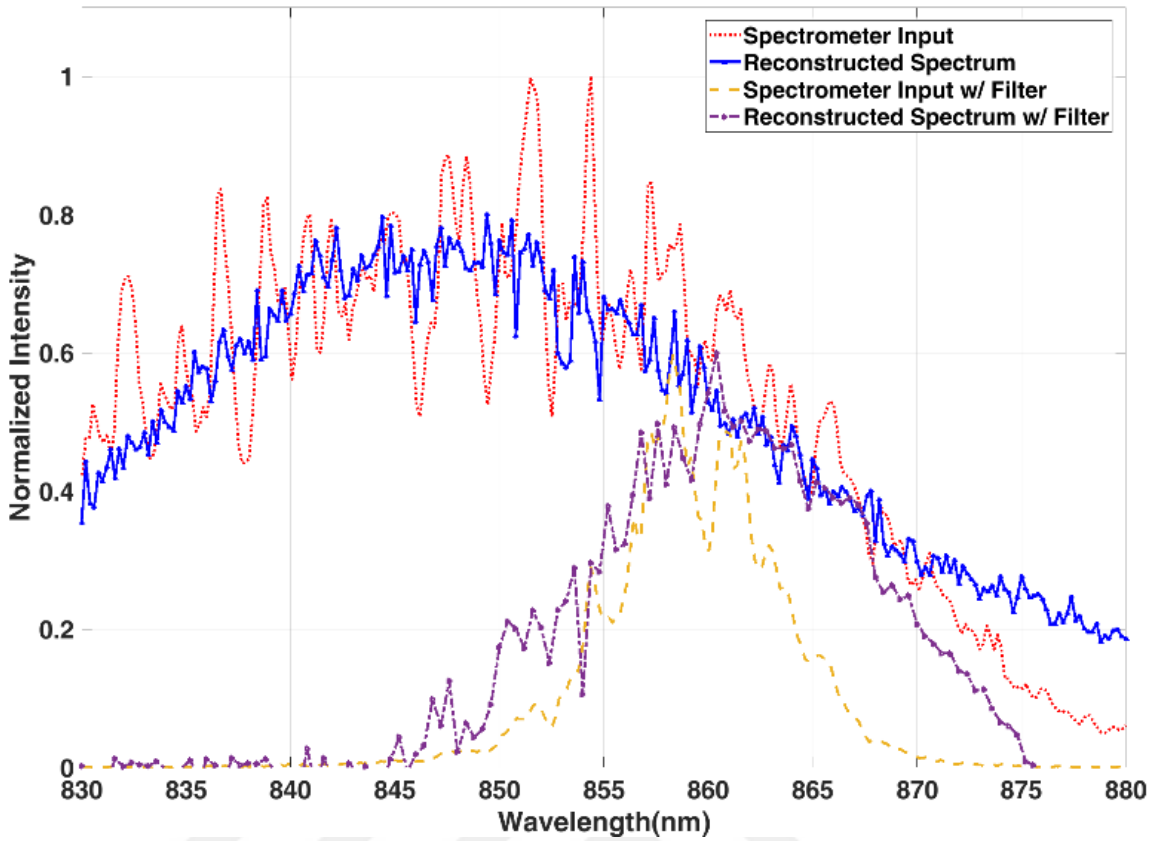

Figure 4.4: Reconstruction of SLD and filtered SLD

5. CONCLUSION

In this work, with the motivation of improving the the resolution and eliminating the tradeoff between resolution and spectral range, a novel spectrometer design is proposed. The design builds upon a prism spectrometer by integating a scattering medium that generates wavelength dependent speckle patterns, this way improving the resolution of a standalone prism spectrometer. The introduced speckle patterns by having a 2D spectral-to-spatial mapping, increase the output space and hence enhancing both the resolution and the spectral range of the spectrometer.

The device is able to differentiate different wavelength by analyzing the rate of decorrelation between the speckle patterns. The seperation between two wavelength components in which the corresponding speckle patterns are uncorrelated gives the resolution of the device. The spectral range of the device is enhanced by exploiting the prism, as it prevents the overlapping of different speckle patterns by dispersing different wavelengths to different horizontal locations on the sensor array. Since the spectral range of a prism is infinite, the realized spectrometer too has a theoretically infinite spectral range, limited by the sensor array area. Thus, the device is adequtely named Speckle Enhanced Prism Spectrometer (SEPS).

Combined, the prism and the speckle pattern analysis offer a powerful spectroscopy tool, eliminating the tradeoff between spectral resolution and spectral range. Although the working principle of the device requires a calibration process, which is prone to noise, to be done before a spectroscopy application, this work demonstrates that with a reasonable level of mechanical and thermal stability the performance of the device is greatly reduced by the noise. In fact an advantage of the calibration process is that the calibration process does not need to be a continuous process as long as the system is stable. It is possible to crate a calibration library, adding different ranges at different points in time, depending on the desired reconstruction range. For this work the SEPS device was operated at NIR region, around 850 nm, but the region of operation can be any wavelength interval, given that calibration can be done in that region.

It was shown that the SEPS device can improve the resolution of a stand alone prism spectorometer by hundredfold without sacrificing spectral range. This resolution can be even further improved by employing a thicker and more concentrated scattering medium. Unfortunately, this enhancement of the scattering medium also increases the amount of out scattered light, leading to a new tradeoff between the light budget and resolution, limiting the resolution improvement for real world applications.

In conclusion, the proposed spectrometer design was able to improve the spectral resolution without limiting the spectral range of a stand alone prism spectrometer. The current set up was able to achieve resolution values in lower picometer ranges in a large spectral region making it possible to use the device in multiple spectroscopy applications that require different wavelength regions.

5.1 Future Work

The current device topology introduces a new tradeoff where light transmission decreases as the scattering medium is enhanced to improve the resolution. This is due to large amount of light waves scattering out of the scattering medium, not reaching the camera. To prevent these outscattering light waves the scattering region can be sandwiched in two reflective surfaces as shown in Figure 5.1, this way redirecting most of the scattered light towards the system. Because the orientation will also be changed, the light will interact with a thicker scattering region. It is presumed that this change of topology will eliminate the trade off between the light budget and resolution, greatly improving the overall performance of the SEPS device.

The SEPS spectrometer is also well suited for OCT applications. OCT is an imaging method that is able to render depth-resolved cross-sectional images of the target, which can be any tissue. Spectral-domain OCT uses a spectrometer to analyze the wavelengths of the reflecting light from the tissue and creating a cross sectional depth image [27]. The resolution of the used spectrometer increases the depth range of the OCT and the spectral range of the spectrometer improves the cross sectional depth resolution of the OCT [28]. Since SEPS eliminates the trade off between the two, it is possible to create an OCT device that is capable imaging high-depth and high-resolution images of tissues.

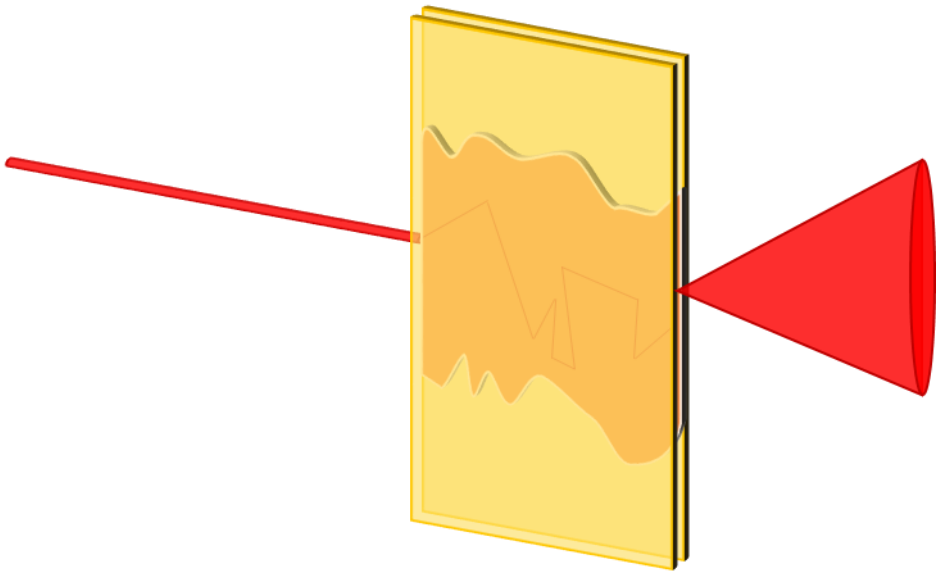

Figure 5.1: The refletive surface (yellow rectangles) added scattering medium placement.

REFERENCES

[1] **B. Meyer and T. Peters, (**2003). “NMR spectroscopy techniques for screening and identifying ligand binding to protein receptors,” Angewandte Chemie - International Edition, vol. 42, no. 8. pp. 864–890.

[2] **O. Beyssac, B. Goffé, J. P. Petitet, E. Froigneux, M. Moreau, and J. N. Rouzaud,** (2003). “On the characterization of disordered and heterogeneous carbonaceous materials by Raman spectroscopy,” in Spectrochimica Acta - Part A: Molecular and Biomolecular Spectroscopy , vol. 59, no. 10, pp. 2267–2276.

[3] **M. Johnck, L. Muller, A. Neyera, and J. W. Hofstraatb,** (2000). “Copolymers of halogenated acrylates and methacrylates for the application in optical telecommunication: optical properties, thermal analysis and determination of unsaturation by quantitative FT-Raman and FT-IR spectroscopy,” Eur. Polym. J., vol. 36, no. 6, pp. 1251–1264.

[4] **R. Leitgeb, M. Wojspectkowski, A. Kowalczyk, C. K. Hitzenberger, M. Sticker, and A. F. Fercher,** (2000) “Spectral measurement of absorption by spectroscopic frequency-domain optical coherence tomography,” Opt. Lett., vol. 25, no. 11, p. 820.

[5] **H. W. Siesler, Y. Ozaki, and S. Kawata,** (2002). Near-Infrared Spectroscopy. Principles, Instruments, Applications, vol. 16, no. 12.

[6] **S. H. Kong, D. D. L. Wijngaards, and R. F. Wolffenbuttel,** (2001). “Infrared micro-spectrometer based on a diffraction grating,” Sensors Actuators, A Phys., vol. 92, no. 1–3, pp. 88–95.

[7] **B. Redding, M. Alam, M. Seifert, and H. Cao,** (2014). “High-resolution and broadband all-fiber spectrometers,” Optica, vol. 1, no. 3, p. 175.

[8] **B. Redding, S. M. Popoff, and H. Cao,** (2013). “All-fiber spectrometer based on speckle pattern reconstruction,” Opt. Express, vol. 21, no. 5, p. 6584.

[9] **N. H. Wan, F. Meng, T. Schröder, R.-J. Shiue, E. H. Chen, and D. Englund,** (2015). “High-resolution optical spectroscopy using multimode interference in a compact tapered fibre,” Nat. Commun., vol. 6, p. 7762.

[10] **B. Redding, S. Liew, R. Sarma and H. Cao,** (2013). "Compact spectrometer based on a disordered photonic chip", Nature Photonics, vol. 7, no. 9, pp. 746-751.

[11] **M. Chakrabarti, M. Jakobsen and S. Hanson,** (2015). "Speckle-based spectrometer", Optics Letters, vol. 40, no. 14, p. 3264.

[12] **Butler, L. R. P.; Laqua, K.** (1995). "Nomenclature, symbols, units and their usage in spectrochemical analysis-IX. Instrumentation for the spectral dispersion and

isolation of optical radiation (IUPAC Recommendations 1995)". Pure Appl. Chem. IUPAC.

[13] **O. Shimizu and J. Watanabe,** (1987). "Polarization spectrophotometer for measurements of both polarized emission and excitation spectra", Review of Scientific Instruments, vol. 58, no. 3, pp. 346-349.

[14] **Brand, John C. D.** (1995). Lines of Light: The Sources of Dispersive Spectroscopy, 1800 - 1930. Gordon and Breach Publishers. pp. 37–42.

[15] **Born, Max; Wolf, Emil** (1999). Principles of Optics. Cambridge: Cambridge University

[16] **Url-1** <*http://www.mathpages.com/home/kmath242/kmath242.htm*> date retrieved 03.10.2018

[17] **Url-2** <*https://www.stellarnet.us/spectrometers/black-comet-hr/*> date retrieved 20.09.2018

[18] **T. Pügner, J. Knobbe and H. Grüger,** (2016). "Near-Infrared Grating Spectrometer for Mobile Phone Applications", Applied Spectroscopy, vol. 70, no. 5, pp. 734-745.

[19] **Dainty C (Ed),** (1984). Laser Speckle and Related Phenomena, Sprinter Verlag, ISBN 0-387-13169-8

[20] **Goodman, J. W.** (1976). "Some fundamental properties of speckle". JOSA. 66 (11): 1145–1150.

[21] **Hahn, David W.** (2009). "Light Scattering Theory" (PDF). University of Florida. Retrieved 20z7-09-22.

[22] **H. Cao,** (2017). "Perspective on speckle spectrometers", Journal of Optics, vol. 19, no. 6, p. 060402.

[23] **J. Dainty,** (1976). "The Statistics of Speckle Patterns", Progress in Optics, vol.

[24] **E. Hecht,** (2001). “Optics 4th edition,” Optics 4th edition by Eugene Hecht Reading MA AddisonWesley Publishing Company 2001, vol. 1. p. 122.

[25] **R. Zawadzki, B. Bower, M. Zhao, M. Sarunic, S. Laut, J. Werner and J. Izatt**, (2005). "Exposure time dependence of image quality in high-speed retinal in vivo Fourier domain OCT", Ophthalmic Technologies XV.

[26] **J. C. A. Barata and M. S. Hussein,** (2012). “The Moore-Penrose Pseudoinverse: A Tutorial Review of the Theory,” Brazilian Journal of Physics, vol. 42, no. 1–2. pp. 146–165.

[27] **Z. Yaqoob, J. Wu and C. Yang,** (2005)."Spectral domain optical coherence tomography: a better OCT imaging strategy", BioTechniques, vol. 39, no. 6, pp. S6-S13.

[28] **B. Povazay, K. Bizheva, A. Unterhuber, B. Hermann, H. Sattmann, A. Fercher, W. Drexler, A. Apolonski, W. Wadsworth, J. Knight, P. Russell, M.**

Vetterlein and E. Scherzer, (2002). "Submicrometer axial resolution optical coherence tomography", Optics Letters, vol. 27, no. 20, p. 1800.

APPENDICES

APPENDIX A: Correlation and Reconstruction MATLAB Source Code

APPENDIX A

Correlation Function

```
function [correl]=correlationFunction(imgMatrix)
% The imgMatrix is a matrix where each row is the each calibration
image
% reshaped into a vactor and

pic_cnt=size(imgMatrix,1);
% initialize the < > components of the equation
top_part=0;
low_part1=0;
low_part2=0;
%loop for each delta lambda
for step=0:(pic_cnt-1)
    step
    for row_no=1:pic_cnt

        if row_no+step>pic_cnt
            break;
        end
        temp_top=imgMatrix(row_no,:).*imgMatrix(row_no+step,:);
        top_part=top_part+temp_top;

        temp_low1=imgMatrix(row_no,:);
        low_part1=low_part1+temp_low1;

        temp_low2=imgMatrix(row_no+step,:);
        low_part2=low_part2+temp_low2;
    end
    step1=step+1;
    divide=pic_cnt-step;

    topp=top_part./divide;
    loww1=low_part1./divide;
    loww2=low_part2./divide;
    loww=loww1.*loww2;

    correl(step1,:)=(topp/loww)-1;
    %reinitialize
    top_part=0;
    low_part1=0;
    low_part2=0;
end
end
```

Reconstruction Function

```
function [outStruct,Strunc,Drep]=spectrumReconstruct(instruct,plotFlag)
% Reconstructs the input Spectrum
% Inputs:
%------------
% instruct : struct that keeps experimental data
% plotFlag : boolean for plotting the spectrum

% Outputs:
%------------
% outStruct: struct that keeps experimental data
% Strunc   : truncated reconstructed spectrum
% Drep     : truncated inverse od singular matrix D

outStruct=instruct;
calibImages=outStruct.calibImages;
inputImage=outStruct.Reconstruct.inputImage;

%amount of spectral channels
M=outStruct.stepCount;

%amount of spatial channels
Nx=size(inputImage,2);
Ny=size(inputImage,1);
N=Nx*Ny;

%% Matrix dimension adjustments
%spatial input image(multi lambda speckle pattern)
I=inputImage;
I=reshape(I,[N,1]);
%tansmission matrix
T=zeros(N,M);

for i=1:M
    tempCalib=calibImages(:,:,i);
    calibColumn=reshape(tempCalib,[N,1]);
    calibColumn=calibColumn./sum(calibColumn);
    T(:,i)=calibColumn;
end
meanSpeckle=mean(mean(T));
sigm=outStruct.sigma;

lambdaAxis=outStruct.lambdaAxis;
probeSpectra=outStruct.Reconstruct.probeSpectra;
probeVals=outStruct.Reconstruct.probeVals;

%no threshold
S=pinv(T)*I;
S=S./max(S);

%single value decomposition
[U,D,V] = svd(T,0);
```

```
%finding the threshold
begin_thresh=(sigm*sqrt(M))/(meanSpeckle*sqrt(M*N));
threshold= max(max(D))*begin_thresh;
%applying the threshold
Dthresh=D;
Dthresh(Dthresh<threshold)=0;
Drep=1./Dthresh;
Drep(~isfinite(Drep))=0;
DrepT=Drep';
% inverse of T
Ttruncinv=V*DrepT*U';
Strunc=Ttruncinv*I;
%normalize
Strunc=Strunc./max(Strunc);

if length(probeVals)~=length(Strunc)
    interpPoints=outStruct.lambdaAxis;
    probeVals=interp1(probeSpectra,probeVals,interpPoints)';
    probeVals(isnan(probeVals))=0;
end

outStruct.Reconstruct.reconVals=Strunc;
outStruct.Reconstruct.threshCoeff=begin_thresh;
outStruct.Reconstruct.Threshold=threshold;

%% Plotting the Reconstruction
if plotFlag
    ff=figure;
    plot(lambdaAxis,probeVals,'r','LineWidth',1.3);
    grid on;
    hold on;
    plot(lambdaAxis,Strunc,'LineWidth',1.3);
    title(['Reconstructed Spectra
threshCoeff=',num2str(begin_thresh),'
[',num2str(length(nonzeros(Drep))),']']);
    xlabel('Wavelength(nm)');
    ylabel('Normalized Intensity');
    legend('Spectrometer Input','Reconstructed Spectrum');
    print(ff,[savefile,'\',num2str(begin_thresh),'.png'],'-dpng','-
r500');
    close(ff);
end
end
```

CURRICULUM VITAE

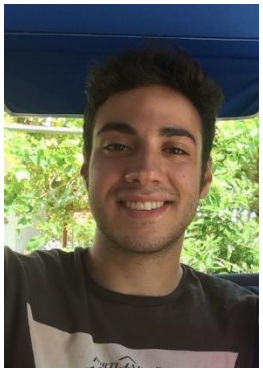

Name Surname **:** Şakir Kaan ÇETİNDAĞ

Place and Date of Birth **:** İzmir – 19.06.1993

E-Mail **:** cetindag.kaan@gmail.com

EDUCATION **:**

- **B.Sc.** **:** 2015, Koç University, Faculty of Engineering, Electric and Electronic Engineering

PROFESSIONAL EXPERIENCE AND REWARDS:

- 2015-2018 Istanbul Technical University Electro-Optic Devices Laboratory (EDL)

PUBLICATIONS, PRESENTATIONS AND PATENTS ON THE THESIS:

- **Çetindağ Ş. K., Toy M. F., Ferhanoğlu O., Çivitci F.** 2018: 20. Ulusal Optik, Elektro-Optik ve Fotonik Çalıştayı – A Modified Prism Spectrometer with High Resolution and Spectral Range, September 14, 2018 Ankara, Turkey.
- **Çetindağ Ş. K., Toy M. F., Ferhanoğlu O., Çivitci F.** 2018. SAÇICI KATMAN İLE ZENGİNLEŞTİRİLMİŞ, YÜKSEK ÇÖZÜNÜRLÜKLÜ PRİZMA TAYFÖLÇERİ. Patent numarası: 2018/10123 – 2018-GE-308811